Received: 30 May 2021 | Revised: 28 June 2021 | Accepted: 29 June 2021

DOI: 10.1002/wnan.1740

FOCUS ARTICLE

WIREs NANOMEDICINE AND NANOBIOTECHNOLOGY WILEY

Ultrasmall superparamagnetic iron oxide nanoparticles: A next generation contrast agent for magnetic resonance imaging

Can Chen[1] | Jianxian Ge[1] | Yun Gao[1] | Lei Chen[1] | Jiabin Cui[1] | Jianfeng Zeng[1] | Mingyuan Gao[1,2]

[1]Center for Molecular Imaging and Nuclear Medicine, State Key Laboratory of Radiation Medicine and Protection, School for Radiological and Interdisciplinary Sciences (RAD-X), Soochow University, Collaborative Innovation Center of Radiological Medicine of Jiangsu Higher Education Institutions, Suzhou, China

[2]Shanghai University of Medicine and Health Sciences (SUMHS), Shanghai, China

Correspondence
Jianfeng Zeng and Mingyuan Gao, Center for Molecular Imaging and Nuclear Medicine, State Key Laboratory of Radiation Medicine and Protection, School for Radiological and Interdisciplinary Sciences (RAD-X), Soochow University, Collaborative Innovation Center of Radiological Medicine of Jiangsu Higher Education Institutions, Suzhou 215123, China.
Email: jfzeng@suda.edu.cn and gaomy@iccas.ac.cn

Funding information
National Key Research and Development Program of China, Grant/Award Number: 2018YFA0208800; National Natural Science Foundation of China, Grant/Award Number: 81720108024; Natural Science Foundation of Jiangsu Province, Grant/Award Number: BK20191418; Nature Science Foundation of Jiangsu Higher Education Institutions of China, Grant/Award Number: 20KJA150006; Priority Academic Program Development of Jiangsu Higher Education Institutions, PAPD; Suzhou Key Industry Technology Innovation Projects, Grant/Award Number: SYG202036

Edited by: Xiangyang Shi, Associate Editor and Gregory Lanza, Co-Editor-in-Chief

Abstract

As a research hotspot, the development of magnetic resonance imaging (MRI) contrast agents has attracted great attention over the past decades for improving the accuracy of diagnosis. Ultrasmall superparamagnetic iron oxide (USPIO) nanoparticles with core diameter smaller than 5.0 nm are expected to become a next generation of contrast agents owing to their excellent MRI performance, long blood circulation time upon proper surface modification, renal clearance capacity, and remarkable biosafety profile. On top of these merits, USPIO nanoparticles are used for developing not only T_1 contrast agents, but also T_2/T_1 switchable contrast agents via assembly/disassembly approaches. In recent years, as a new type of contrast agents, USPIO nanoparticles have shown considerable applications in the diagnosis of various diseases such as vascular pathological changes and inflammations apart from malignant tumors. In this review, we are focusing on the state-of-the-art developments and the latest applications of USPIO nanoparticles as MRI contrast agents to discuss their advantages and future prospects.

This article is categorized under:

Diagnostic Tools > In Vivo Nanodiagnostics and Imaging

KEYWORDS

contrast agents, iron oxide nanoparticles, magnetic resonance imaging, ultrasmall

Can Chen and Jianxian Ge contributed equally to this study.

1 | INTRODUCTION

Magnetic resonance imaging (MRI) has been demonstrated to be one of the most important and powerful imaging techniques in clinical diagnosis due to its non-invasiveness, high spatial resolution, and no ionizing radiation nature (Koenig & Kellar, 1995; Lee & Hyeon, 2012; Na & Hyeon, 2009). As the relaxation times of different tissues often overlap, enhancing the imaging contrast particularly that between the benign and malignant tissues has been becoming one of the important subjects for MRI. Following this need, versatile MRI contrast agents are being created.

In fact, the MRI contrast agent itself does not produce a signal, but it changes the relaxation efficiency of water protons close-by to improve the imaging contrast. To this end, two types of MRI contrast agents, that is, T_1 (or positive) contrast agents and T_2 (or negative) contrast agents, are developed accordingly. T_1 contrast agents are usually coordination compounds or inorganic nanoparticles containing paramagnetic metal ions (with unpaired electrons), which can accelerate the longitudinal relaxation of protons, thereby producing brighter MR images, while T_2 contrast agents are usually superparamagnetic iron oxide (SPIO) nanoparticles which can effectively shorten the transverse relaxation time of protons, thus generating darker MR images. So far, a variety of MRI contrast agents have been reported and used in preclinical and clinical studies, including gadolinium (Gd)-based contrast agents (GBCAs), manganese (Mn)-based contrast agents, and iron oxide-based contrast agents. Among these MRI contrast agents, GBCAs are the most prevalent T_1 contrast agents in the clinic, such as Magnevist (Gd-DTPA), ProHance (Gd-DO3A-HP), Omniscan (Gd-DTPA-BMA), Dotarem (Gd-DOTA), Eovist (Gd-EOB-DTPA), and Optimark (Gd-DTPA-BMEA) (Caspani et al., 2020). However, due to potential risk of nephrogenic systemic fibrosis (NSF) caused by the free Gd^{3+} ions, GBCAs, that is, Magnevist, Omniscan, and Optimark are considered as "high risk" by the US Food and Drug Administration (FDA), especially for patients with acute kidney injuries or severe renal diseases. In addition, Gd^{3+} deposition in the human brain is another noticeable adverse effect of GBCAs, for example, Omniscan (McDonald et al., 2015). Besides, the short blood circulation time of small-molecule GBCAs limits their applications in high-resolution MRI that require long scan window. Mn-based T_1 contrast agents include Mn-chelates (e.g., Mn-DPDP), Mn-containing nanoparticles, and manganese oxide nanoparticles (e.g., MnO, MnO_2, Mn_3O_4, and MnO_x) (Cai et al., 2019; Zeng et al., 2017). However, the application of Mn-based contrast agents is limited by possible occurrence of neurodegenerative diseases due to the brain accumulation and toxicity of free Mn^{2+} ions (Kamer et al., 2018; Reaney et al., 2006). Compared with Gd/Mn-based contrast agents, iron oxide nanoparticles-based contrast agents are considered more biocompatible because iron is an essential element of the human body and an indispensable part of hemoglobin (Z. Y. Gao et al., 2015; Jin et al., 2014; Lee et al., 2015; Zeng, Jia, et al., 2014). SPIO nanoparticles are widely known as T_2 contrast agents in the clinic for their ability to shorten T_2 relaxation time (Z. Y. Gao et al., 2015; J. C. Li et al., 2014; R. R. Qiao et al., 2009). Nevertheless, the applications of SPIO as liver-specific T_2 contrast agents are widely adopted owing to the passive accumulation of SPIO nanoparticles in liver. In addition, the dark signal of T_2 contrast agents may be interfered by the background signals such as bleeding, calcification, or metal deposition, which may mislead clinical diagnosis (Bietenbeck et al., 2015; Daldrup-Link, 2017). Moreover, the "blooming effect" induced by T_2 contrast agents can enlarge the imaging area and may further reduce the resolution of T_2-weighted MRI because of the disturbance of local magnetic field caused by the high magnetic moment of T_2 contrast agents (Kim et al., 2011; Lee et al., 2011). In contrast, T_1-weighted MRI can provide more accurate high-resolution imaging and thus becomes more favorable than T_2-weighted MRI in the clinic.

In recent years, ultrasmall SPIO (USPIO) nanoparticles with a core diameter smaller than 5.0 nm have received increasing attention as MRI contrast agents because they present both outstanding T_1-weighted MRI performance and excellent biocompatibility (Bao et al., 2018; Marco et al., 2007; Shen, Wu, & Chen, 2017; Zhao et al., 2014). With the decrease of particle size, USPIO nanoparticles exhibit lowered magnetization due to the spin-canting effect, so they can effectively shorten T_1 relaxation time of water protons and are suitable for enhancing T_1-weighted MRI. Furthermore, the ultrasmall size endows the USPIO nanoparticles with the following advantages: (1) they can escape the nonspecific uptake of mononuclear phagocytes to achieve long-term circulation, which is conducive to the targeted imaging, steady-state imaging, as well as high-resolution imaging; (2) they are renal clearable upon proper surface modification and thus can reduce the risk of iron overload especially for patients with iron metabolism diseases to show better biocompatibility and biosafety; (3) they are suitable for generating T_2/T_1 switchable contrast enhancement effects via assembly/disassembly for improving the sensitivity and accuracy of MRI. In view of these unique advantages, a variety of USPIO-based MRI probes have been designed for the diagnosis of various diseases. Herein, we comprehensively compare USPIO with both Gd/Mn- and SPIO-based MRI contrast agents, combining the recent progress, to discuss about the current status and future prospects of USPIO as a new generation of MRI contrast agent.

2 | ADVANTAGES OF USPIO NANOPARTICLES

2.1 | Outstanding MRI performance

USPIO is composed of an ultrasmall inorganic iron oxide core and an organic surface shell, which is normally used as T_1 contrast agent in contrast to SPIO that has a larger core and is widely accepted as T_2 contrast agent. The core size of iron oxide particles strongly determines their relaxation properties. Nevertheless, the surface structure also plays important roles which are elucidated by the inner/outer sphere models (Bai et al., 2018; Jeon et al., 2020; Ni et al., 2017; Shen, Chen, et al., 2017). The inner sphere model tells that reducing the particle size is in favor of high longitudinal relaxivity (r_1), because the specific surface area increases as the particle size decreases, and thus the water protons can effectively interact with more iron ions of small particles. The outer sphere model, however, argues that reducing the particles size will decrease the magnetization and lower the transversal relaxivity (r_2), because the volume of the ordered spin is decreased with the decrease of particle size (Shin et al., 2015; Zhou et al., 2019). Therefore, USPIO becomes extraordinarily suitable for T_1-weighted MRI owing to the high r_1 value and the small r_2/r_1 ratio (C. L. Liu et al., 2014).

Kim et al. compared the magnetic properties of differently sized USPIO particles, that is, 1.5, 2.2, and 3.0 nm, with SPIO nanoparticles of 12 nm and found that the magnetization of iron oxide particles drops as the diameter decreases, especially for the USPIO (Figure 1(a)) (Kim et al., 2011). The low magnetization of USPIO can be attributed to the enhanced spin-canting effect owing to the small core size (Figure 1(b)). For example, the calculated spin-canting ratio increased from 38.6% for 12 nm SPIO to 93.6% for 3.0 nm USPIO and further to 99.4% for 2.2 nm USPIO. As expected, USPIO of 3.0 nm gives rise to bright MRI images, while SPIO of 12 nm produces negative contrast, as shown in Figure 1(c). However, it is not always that the smaller the particle size, the higher the r_1 value and stronger the T_1 contrast enhancement. In order to find the optimal size for T_1-weighted MRI, Shen et al. synthesized a series of size controllable USPIO of 1.9, 2.6, 3.3, 3.6, 4.2, 4.8, and 4.9 nm to find out the particle size dependency of r_1 and r_2/r_1 as well (Shen, Chen, et al., 2017). Obviously, the r_1 value increases firstly and decreases against the particle size, while r_2/r_1 presents a reverse tendency, giving rise to an optimal size of 3.6 nm for T_1 contrast enhancement, as shown in Figure 1(d),(e). The non-monotonic particle size dependency of r_1 is probably caused by the overall effects of inner/outer spheres that affect r_1 oppositely.

Although the magnetization of USPIO particles largely decreases with the decrease of particle core size, they may still exhibit strong T_2 enhancement ability if the core size is appropriately controlled, leading to T_1/T_2 dual-modal imaging contrast agents (X. Ma et al., 2019; G. Wang et al., 2016). For example, Gao group has developed polyethylene glycol (PEG)-coated iron oxide nanoparticles (Hu et al., 2011). A high-performance T_1/T_2 dual-modal MRI contrast agent with r_1 of 19.7 mM^{-1} s^{-1} and r_2 of 39.5 mM^{-1} s^{-1} under 1.5 T was obtained. The excellent dual-modal contrast enhancement effects may be attributed to the suitable core size (5.4 nm) and high saturation magnetization (94 emu g^{-1}), the latter of which was mainly related to high crystallinity and surface coating. Li et al. reported USPIO of 3.3 nm showing r_1 of 8.3 mM^{-1} s^{-1} and r_2 up to 35.1 mM^{-1} s^{-1} under 4.7 T, better than those of the clinical T_1 contrast agent Gd-DTPA (r_1 = 4.8 mM^{-1} s^{-1} and r_2 = 5.3 mM^{-1} s^{-1}) and the commercial SPIO-based contrast agent SHU-555C (r_1 = 2.9 mM^{-1} s^{-1} and r_2 = 69 mM^{-1} s^{-1}) (Z. Li et al., 2012).

As aforementioned, the core size of magnetic iron oxide nanoparticles exhibits opposite impacts on r_1 and r_2. It is difficult to pursue simultaneously high r_1 and high r_2 simply by varying the particle size. To solve this problem and uncover the effects of surface ligands on magnetic properties, Gao group prepared 3.6 nm and 10.9 nm iron oxide nanoparticles coated with PEGs bearing different anchoring groups such as diphosphate (DP), hydroxamate (HX), and catechol (CC) group, respectively (Figure 1(f)) (Zeng, Jing, et al., 2014). It was demonstrated that 3.6 nm USPIO coated with HX-PEG and CC-PEG presented higher r_1 and r_2 than those modified with DP-PEG (Figure 1(g)), which was explained by the affinity of the surface ligands that affected the magnetization of particles and the conjugated structure of the anchoring groups that increased the inhomogeneity of the local magnetic field to enhance the T_2 contrast effect. In addition, the particle surface coating structure can also remarkably affect the relaxation properties of the nanoparticles due to its strong correlation with the retention time and the number of coordinated water molecules in the inner layer (Bai et al., 2018; C. L. Liu et al., 2014; Sherwood et al., 2017; Xie, Wang, et al., 2020). For instance, Xiao et al. found that USPIO particles with different core size of 4.8–7.3 nm but similar hydrodynamic size of 9.9–14 nm and r_2/r_1 ratios of 3.9–4.1 could also present different T_1 contrast enhancement effects, for example, r_1 of 15.9–18.8 mM^{-1} s^{-1} for particles coated with surface ligand bearing a linear PEG segment and 5.3 mM^{-1} s^{-1} for those coated with surface ligand bearing a brushed-PEG segment (Xiao et al., 2018). It was speculated that the slightly dense surface coating formed by the brushed-PEG ligand would hinder the interaction between paramagnetic iron ions on particle surface and surrounding water protons to reduce the r_1 value.

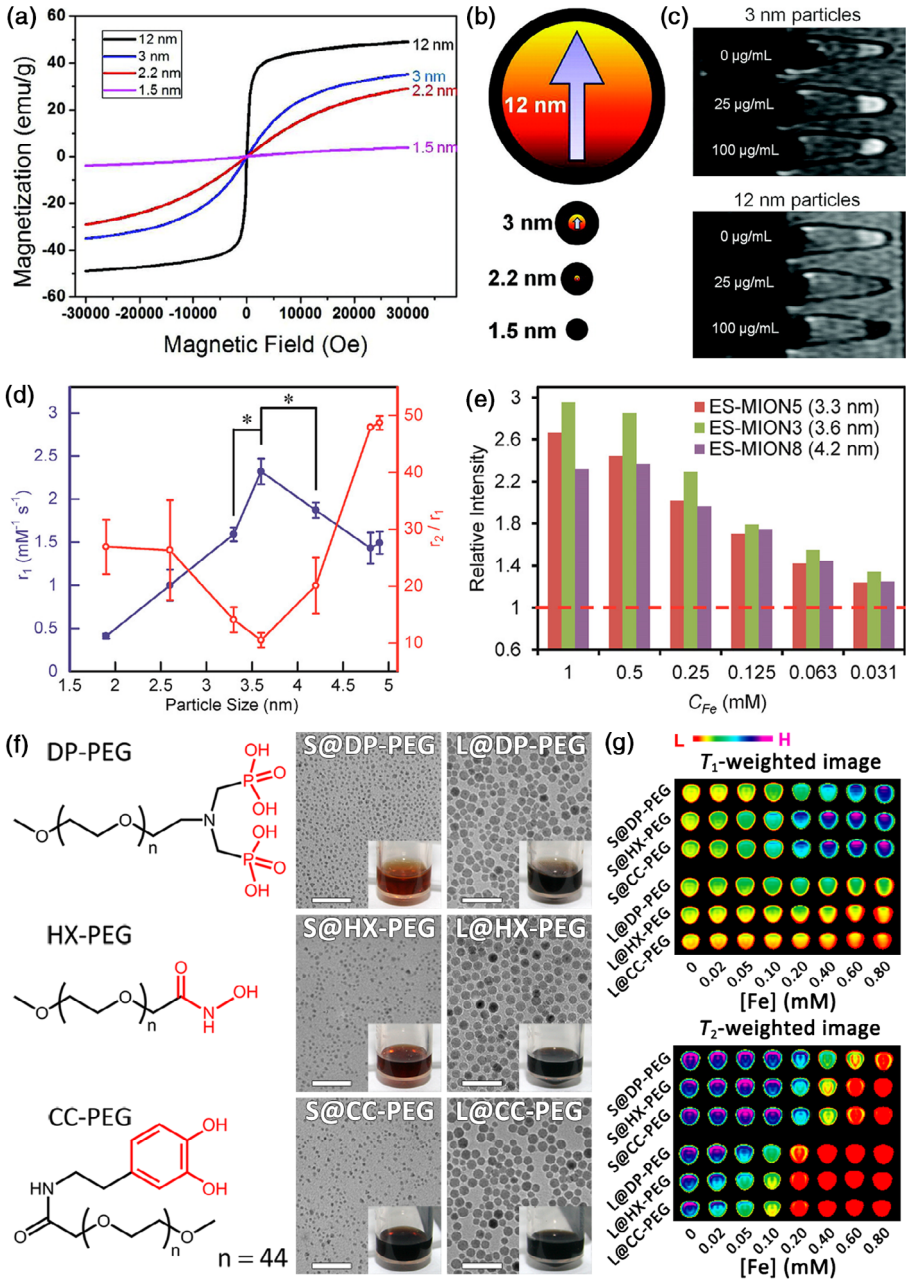

FIGURE 1 (a) Field-dependent magnetization curves of differently-sized USPIO nanoparticles at 300 K; (b) illustration of the spin canting effect of USPIO particles with different diameters; (c) T_1-weighted MRI of MCF-7 cell pellets after 24 h incubation with 3.0 nm and 12 nm iron oxide nanoparticles, respectively (Reprinted with permission from Kim et al., 2011, Copyright 2011, American Chemical Society); (d) particle size dependencies of r_1 value and r_2/r_1 ratio; (e) the corresponding T_1 MR signal intensities of USPIO nanoparticles against Fe concentration (Reprinted with permission from Shen, Chen, et al., 2017, Copyright 2017, American Chemical Society); (f) chemical structures of the anchoring groups of three PEG-based ligands and the corresponding TEM images of 3.6 nm nanoparticle (S) and 10.9 nm nanoparticle (L) stabilized by these three PEG ligands, respectively; and (g) T_1/T_2-weighted MR images of solutions containing these two differently sized PEGylated particles (Reprinted with permission from Zeng, Jia, et al., 2014, Copyright 2014, Wiley). MCF-7, human breast cancer cells; MRI, magnetic resonance imaging; PEG, polyethylene glycol; TEM, transmission electron microscope; USPIO, ultrasmall superparamagnetic iron oxide

In order to improve the accuracy of MRI in practice, versatile strategies have been proposed to prepare T_1/T_2 dual-modality imaging contrast agents, although some USPIO particles present dual-modal MRI functions. Magnetic iron oxide particles and Gd/Mn-chelates are representative T_2 and T_1 contrast agents, respectively, therefore, integrating them together becomes a straightforward approach for producing T_1/T_2 dual-modal contrast agents (Huang et al., 2014; Shin et al., 2014). For example, Yang et al. reported such a contrast agent constructed by covalently linking silica-coated

SPIO with paramagnetic Gd-DTPA (H. Yang et al., 2011). The r_1 value was found to increase significantly against Gd content, while the r_2 value was simultaneously decreased, indicating that Gd may interfere with the T_2 relaxation process of SPIO. Even though the resulting contrast agents exhibited dual-modal T_1/T_2 imaging contrast enhancement effects, the above approach is defective due to the existing issues rooted in colloidal instability, composition-dependent r_1/r_2 ratio as well as difficulties in further surface functionalization. Furthermore, the potential toxicity of the leaked Gd^{3+} and Mn^{2+} is also problematic for further clinical applications.

The controllable assembly of USPIO particles formed upon stimulations with pH (Cao, He, et al., 2020; Jia et al., 2021) and glutathione (GSH) (Cao, Mao, et al., 2020) has been demonstrated to be able to provide T_1/T_2 switchable contrast agents that are different from the above-mentioned T_1/T_2 dual-modality contrast agents that simultaneously show T_1- and T_2-weighted imaging contrast enhancement effects. For instance, Li et al. reported pH-sensitive USPIO nanoparticles that are assembled through pH-responsive hydrazone bonds (—C═N—N—) for T_1-weighted MRI of tumors (F. Li, Liang, et al., 2019). In neutral pH environment, the assembled particles presented enhanced T_2-weighted signals, while they fell apart in acidic tumor microenvironment to give rise to strong T_1-weighted MR signal. Recently, Gao group constructed a GSH-responsive MRI probe that can be switched from T_1 to T_2 enhancement due to the GSH-induced aggregation of the USPIO particles within tumors, which was further demonstrated possible for quantitatively mapping the endogenous GSH in intracranial tumors through MRI (Zhang et al., 2021). In detail, USPIO particles of 3.9 nm simultaneously bearing surface maleimide groups and functional peptide sequences were designed to obtain the probe that displayed a strong T_1 contrast enhancement effect in the absence of GSH. However, it exhibited dramatically enhanced T_2 enhancement in GSH-rich environment as GSH can reduce the disulfide bonds embedded in the peptide sequence to generate thiol groups that react with the maleimide groups from the adjacent USPIO particles to glue them together. It was further demonstrated that such GSH-induced particle aggregation could give rise to interlocked T_1 and T_2 signal variations, which were proven to quantitatively correlate with GSH concentration to enable the GSH mapping of intracranial tumor in vivo (Zhang et al., 2021).

As discussed above, some key factors including size, surface properties, and aggregation status have been adopted to adjust the relaxivities of USPIO to give rise to outstanding T_1 or T_1/T_2 switchable MRI properties. Apart from the inherent properties of the USPIO itself, the effects of external magnetic field strength on the contrast enhancement performance cannot be ignored. Deng et al. studied the magnetic field (0.5, 1.5, and 3.0 T) dependent relaxivities of USPIO (L. H. Deng et al., 2021). They found that increasing magnetic field strength will suppress the r_1 effect, but slightly increase the r_2 effect of magnetic iron oxide particles, resulting in a sharp rise in r_2/r_1 ratio. Therefore, 4.0 nm USPIO exhibiting good T_1 contrast enhancement performance at 0.5 and 1.5 T showed excellent T_1/T_2 dual-modal contrast enhancement ability at 3.0 T.

2.2 | Long blood circulation time

In general, nanoparticle-based MRI contrast agents particularly SPIO particles tend to be recognized and phagocytized by the reticuloendothelial system (RES), while the small molecule-based ones are usually rapidly cleared through kidney after intravenous delivery. Both of these two typical pharmacokinetic behaviors will shorten the blood circulation time, which is unfavorable for acquiring a high-quality contrast MRI. In difference, USPIO shows a relatively long blood circulation time owing to the appropriate size which is beneficial for suppressing the RES uptake, at the same time facilitates the renal clearance. Deng et al. showed that 4.0 nm PEGylated USPIO could provide more than 2 h long contrast-enhanced angiography, while the 8.0 nm counterpart with the same surface modification could only provide 30 min enhancement and Gd-DTPA enhancement lasted just for several minutes (L. H. Deng et al., 2021).

Similar to the intensively investigated SPIO, the appropriate surface functionalization of USPIO is necessary for improving the antifouling ability to resist the nonspecific adsorption of proteins and other biological macromolecules, thereby extending blood residence time. PEG (S. Liu et al., 2010) and zwitterionic molecules (Pombo-García et al., 2017) such as L-cysteine (L-Cys) (P. Wang, Yang, et al., 2017) and zwitterionic dopamine sulfonate (ZDS) (Zhou et al., 2013) were used for such purpose. Sandiford et al. revealed that the nearly neutral surface potential of −1.24 mV provided by PEG coatings and the high PEG density could work together to minimize the opsonization of USPIO and suppress the following RES uptake (Sandiford et al., 2013). As they expected, the PEGylated USPIO of 5.5 nm presented a blood half-life up to 3.0 h. In addition, Ma et al. demonstrated that the L-Cys modification through a PEG spacer effectively increased blood half-life of 2.8 nm USPIO from 2.1 to 6.2 h, as shown in Figure 2 (a) (D. Ma et al., 2017).

Prolonging the blood circulation time of USPIO is of great significance. First of all, the long blood half-life is favorable for improving the accumulation efficiency of the imaging probe at the disease site. For example, 3.0 nm USPIO showed a higher accumulation in tumor than 10 nm and 20 nm SPIO counterparts due to the prolonged half-life up to 10 h, as shown in Figure 2(b) (L. Wang, Huang, et al., 2017). In addition, the long blood circulation time of USPIO will allow a prolonged temporal scanning window for acquiring high spatial resolution MRI. Shin et al. found that USPIO with a hydrodynamic diameter (HD) of 5.0 nm possessed stronger angiographic signal than Gd-DOTA at both their first pass and steady state, thus gaining a longer temporal scanning window (Shin et al., 2021). To reveal the relationship between the scanning time and MRI resolution, a spatial resolution model composed of capillaries with various sizes ranging from 100 to 1000 μm was constructed. As shown in Figure 2(c), 10 min scanning gives rise to a spatial

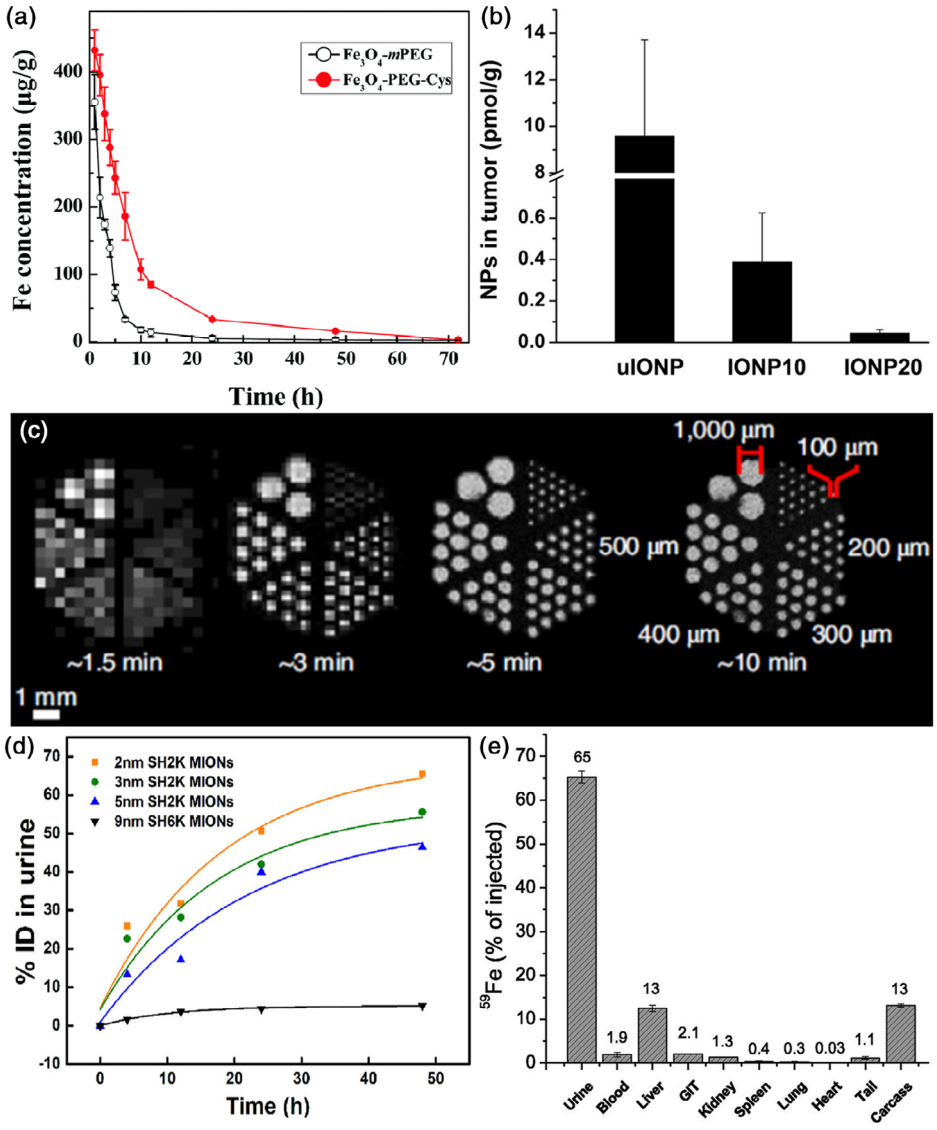

FIGURE 2 (a) Blood circulation behaviors of USPIO-PEG nanoparticles and L-Cys modified USPIO-PEG nanoparticles (Reprinted with permission from D. Ma et al., 2017, Copyright 2017, The Royal Society of Chemistry); (b) iron contents in tumor tissues harvested from mice receiving intravenous injections of differently-sized iron oxide nanoparticles, respectively (Reprinted with permission from L. Wang, Huang, et al., 2017, Copyright 2017, American Chemical Society); (c) the scanning time-dependent spatial resolution of MRI (Reprinted with permission from Shin et al., 2021, Copyright 2021, Springer Nature); (d) the renal clearance curves of iron oxide nanoparticles with different hydrodynamic sizes (Reprinted with permission from Xie, Wang, et al., 2020, Copyright 2020, American Chemical Society); (e) biodistribution of ZDS-coated USPIO particles labeled with ^{59}Fe in mice (Reprinted with permission from Wei et al., 2017, Copyright 2017, National Academy of Sciences). L-Cys, L-cysteine; MRI, magnetic resonance imaging; PEG, polyethylene glycol; USPIO, ultrasmall superparamagnetic iron oxide; ZDS, zwitterionic dopamine sulfonate

resolution as high as 100 μm under 3.0 T MRI, while ~1.5 min scanning generates a much lower spatial resolution of about 1000 μm. In this context, USPIO holds an opportunity to provide a better spatial resolution than Gd-DOTA for MRI. Therefore, small particle size and appropriate surface modification are jointly in favor of bioavailability and imaging resolution for achieving accurate diagnosis.

2.3 | Renal clearance

According to the requirements of FDA, all injected contrast agents should be completely cleared from the body within a reasonable period of time for clinical translation (Choi et al., 2007). Renal clearance is advisable for nanoparticles as it helps reduce the unwanted retention in nontargeted tissues after intravenous delivery (Ehlerding et al., 2016; Xie, Xu, et al., 2020; Zhou et al., 2020). Therefore, renal clearable contrast agents possess enormous superiority with respect to clinical translations. Typically, it is believed that USPIO with a HD below the threshold of renal glomerular filtration (6.0–8.0 nm) can be effectively cleared from the circulatory system through bladder and urine (J. Liu et al., 2013). However, to obtain such an ultrasmall HD, appropriate surface modification becomes essential in addition to properly controlling the core size. Moreover, the surface modification structure strongly determines the colloidal stability and antifouling ability, both of which critically regulate the clearance pathway of the intravenously delivered particles. The long-chain PEGs, silica coating, hydrophilic surface modification with polymeric surfactants have been widely adopted to increase the biocompatibility and prevent the serum protein adsorption. However, the HD of resulting nanoparticles modified by the above surface coating often exceeds 10 nm.

Thus, aiming at facilitating renal clearance, various small-ligands were developed to modify USPIO nanoparticles. For instance, Xie et al. reported a low molecular weight succinylated heparin (SH) for coating USPIO particles of 2.0, 3.0, and 5.0 nm to obtain particles with HD of 6.0, 6.8, and 8.1 nm, respectively (Xie, Wang, et al., 2020). As shown in Figure 2(d), they further observed that the renal excretion rate, that is, 65.6%, 55.7%, and 49.5% determined via inductively coupled plasma-mass spectrometry at 48 h postinjection, was inversely correlated with the HD. When the HD was increased to 13.5 nm by coating 9.0 nm particles with the same SH, no renal clearance was observed. ZDS modification is also suitable for obtaining small HD. For example, Wei et al. developed USPIO with a HD of 4.7 nm by coating 3.0 nm particles with ZDS (Wei et al., 2017). Through the following ^{59}Fe-radiolabeling, the biodistribution in mice was obtained as shown in Figure 2(e). It turned out that 65% of the injected USPIO nanoparticles were cleared through the kidney within 4.0 h. Shin et al. gave another creative shot at renal clearable USPIO by controlling the overall size and charge by growing an amorphous-like hydrous ferric oxide on a polysaccharide supramolecular core (Shin et al., 2021). The bright enhancement of ureters and bladder illustrated that USPIO nanoparticles in the blood vessels were filtered by the kidney, gathered in the bladder, and finally excreted through the urinary tract. By quantitatively monitoring the content of USPIO in the urine, it was found that 92% of the USPIO nanoparticles were excreted within 8.0 h after intravenous injection, and ~100% of the USPIO nanoparticles were cleared after 24 h, indicating that the USPIO nanoparticles were completely excreted by kidney filtration within 1 day. They finally concluded that the ultrasmall HD of ~5.0 nm and slightly negative charge of −2.9 mV could in some ways preclude USPIO from binding serum proteins and further accumulating in the mononuclear phagocytic system, thereby collectively facilitating the renal clearance.

2.4 | Excellent biosafety

The short- and long-term biocompatibility as well as biosafety profile of USPIO nanoparticles have been evaluated at different levels, including cell level such as human macrophages (Feng et al., 2010; Lunov et al., 2010; Saito et al., 2012), hepatocytes (He et al., 2018), stem cells (Hao et al., 2019; Ledda et al., 2020), coronary artery endothelial cells (Palacios-Hernandez et al., 2020), and neural precursor cells (Eamegdool et al., 2014), small animal level such as mice (Ledda et al., 2020; Stanicki et al., 2014) and rats (Garcia-Fernandez et al., 2020), and large animal level such as rabbits, beagle dogs, and macaques (Y. Lu et al., 2017; Rui et al., 2016). No obvious acute or chronic toxicity was observed. For instance, Shin et al. explored the biocompatibility of USPIO composed of a polysaccharide supramolecular core and hydrous ferric oxide shell in rats (Shin et al., 2021). In the acute toxicity test, no abnormality in the survival, behavior or the histopathological analysis was observed after intravenous injection of the probe with dose up to 35 mg Fe/kg body weight. Similarly, Lu et al. found that the cytotoxicity of PEGylated USPIO on human umbilical vein

endothelial cells and human periodontal ligament stem cells was low enough to be ignored (Y. Lu et al., 2017). The further biosafety test in nonhuman primate macaques exhibited no death or adverse symptom after the intravenous injection of USPIO (10 mg Fe/kg body weight) over 3-month observation. Moreover, the hematological and serum biochemical indexes of the macaques kept normal, indicating an excellent biocompatibility of USPIO on nonhuman primates.

In order to show the biosafety of USPIO as T_1 contrast agent, Chen et al. compared it with manganese oxide nanoparticles (e.g., MnO NPs) and GBCAs (e.g., gadopentetate dimeglumine injection [GDI]) in mouse (R. Chen et al., 2015). The total safety assessment on all three contrast agents was summarized and given in Figure 3(a). USPIO nanoparticles with dose of 10 mg Fe/kg body weight exhibited the best biosafety profile with just one side effect of endoplasmic reticulum stress on spleen. In contrast, GDI was obviously injurious to kidney due to the high accumulation in renal tissue with significantly increased tumor necrosis factor-α and interleukin-6 presented in serum, while MnO NPs were considered highly toxic because they induced a large number of adverse reactions. The same group further assessed the toxicological risk of USPIO in renal failure rats to prove the feasibility of substituting GBCAs (e.g., gadodiamide) with USPIO in clinical MRI diagnosis of patients with renal diseases (Weng et al., 2019). As shown in Figure 3(b), only the gadodiamide-treated groups exhibited severe NSF symptoms that were probably related to the dermatic Gd accumulation which could promote the activation of macrophages and the secretion of pro-inflammatory cytokines to eventually induce the fibrosis pathway. Nevertheless, the USPIO-treated groups indicated a low risk of NSF because there was neither activation of macrophages nor expression of profibrotic genes with dose up to 20 mg

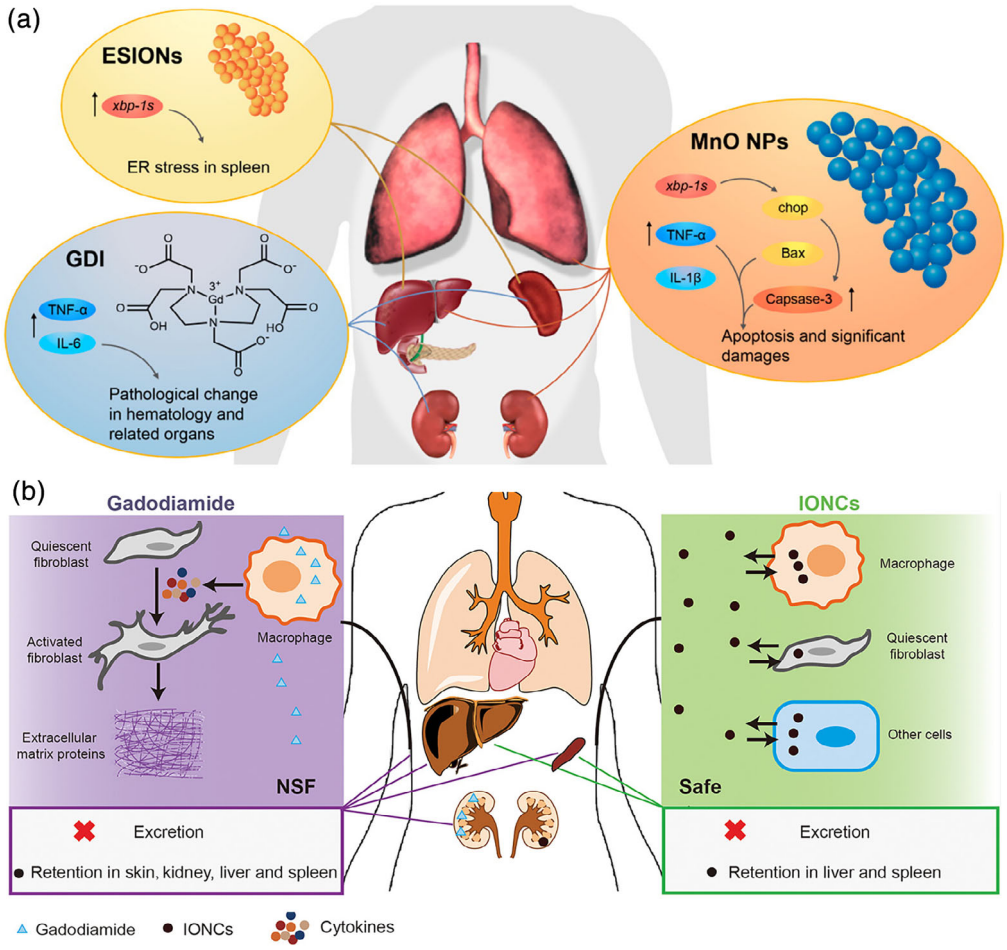

FIGURE 3 (a) The biological effects of USPIO-, Gd- and Mn-based T_1 MRI contrast agents delivered through intravenous injection (Reprinted with permission from R. Chen et al., 2015, Copyright 2015, American Chemical Society); (b) toxicological risk assessments of USPIO- and Gd-based T_1 MRI contrast agents in renal failure rats (Reprinted with permission from Weng et al., 2019, Copyright 2019, American Chemical Society). Gd, gadolinium; Mn, manganese; MRI, magnetic resonance imaging; PEG, polyethylene glycol; USPIO, ultrasmall superparamagnetic iron oxide

Fe/kg body weight. In a word, the above studies have clearly demonstrated the potential of USPIO nanoparticles as the next generation of clinical T_1 MRI contrast agent, but standardized methodologies remain to be developed for fully depicting the biosafety profile of USPIO nanoparticles before their clinical application.

3 | APPLICATIONS OF USPIO NANOPARTICLES

The blood circulation time and biodistribution are needed to be specifically considered for the subsequent applications. In this context, long blood circulation time and reduced organ accumulation of USPIO nanoparticles undoubtedly make them potent candidates for a wide range of MRI applications, for example, blood pool imaging (Sandiford et al., 2013; Tromsdorf et al., 2009; Wei et al., 2017), tumor imaging (Du et al., 2020; D. Liu et al., 2020; Shi et al., 2020; Song et al., 2013; C. Yang et al., 2019; Zhang et al., 2020), atherosclerosis imaging (Alam et al., 2015; Ruetten et al., 2020; Usman et al., 2015), and inflammation imaging (Abbas et al., 2020; Lagan et al., 2020; Luo et al., 2020).

3.1 | Blood pool imaging

Blood pool imaging plays an important role in clinical MRI because of its effective detection of multiple blood-related diseases including myocardial infarction, renal failure, atherosclerotic plaque, thrombosis, tumor angiogenesis, and so on. Basically, the prerequisite of given contrast agents for effective blood pool imaging is that the contrast agents must have a sufficiently long blood residence time that is one of the unique features of USPIO nanoparticles (Gharehaghaji et al., 2015; Thrippleton et al., 2019). Kim et al. demonstrated the potential of 3.0 nm PEG-derivatized phosphine oxide-capped USPIO nanoparticles for blood pool imaging, which presented a high r_1 value of 4.78 mM^{-1} s^{-1} and a low r_2/r_1 ratio of 6.12 under 3.0 T (Kim et al., 2011). Unlike Gd-DOTA, the USPIO nanoparticles showed an excellent performance in high-resolution blood pool MRI, allowing the clear observation of various blood vessels with diameter down to 0.2 mm. The excellent performance of PEG-coated USPIO was also observed by Lu et al. in large animals including beagle dogs and macaques for magnetic resonance angiography (MRA) using a clinical 3.0 T MR scanner (Y. Lu et al., 2017). The high-resolution arterial angiography results, as shown in Figure 4, clearly demonstrated that USPIO is very suitable for small arteries imaging.

Theoretically, the resolution of MRI is closely related to the intensity of magnetic field. High magnetic field is in favor of high spatial resolution and signal-to-noise ratio (SNR) (Duyn et al., 2007). Wang et al. reported an excellent contrast agent composed of a 2.3 nm USPIO core and a PEG shell covalently attached through citric acid on the particle surface for MRI under 7.0 T (J. Wang et al., 2021). They observed high T_1 contrast enhancement which was explained by the interactions between USPIO and the surrounding water protons via uncoordinated carboxyl groups of citric acid on the particle surface. High-resolution imaging of cerebral vessels with pretty small diameters, for example, the middle meningeal artery of approximately 140 μm was achieved with the USPIO probe. In difference, the Gd-DTPA and 20 nm SPIO counterpart presented weak contrast enhancement that faded within 15 min. Recently, Shin et al. reported MRA studies of USPIO particles under 9.4 T (Shin et al., 2021). In their study, the innovative contrast agent formed by polysaccharide supramolecular core and an amorphous-like iron oxide patched shell as mentioned above was prepared. The excellent T_1 enhancement effect of resulting particles was attributed to the facts that water molecules surrounding the particles are easily accessible to the surface ferric ions and the iron oxide component exhibits low magnetization. In consequence, as shown in Figure 4, blood vessels including the brain vessels, peripheral vessels, and coronary vessels of rodents, and lower limb vessels of rabbits were successfully visualized, even for those with diameter down to 100 μm, demonstrating great potential of USPIO probe for clinical applications.

3.2 | Tumor imaging

The enhanced permeability and retention (EPR) effect mediated by tumor vascular leakage is commonly considered as the main reason for nanoparticles to enrich in the tumor site, providing nanoobjects with tumor passive targeting ability. In this context, long blood circulation time will surely provide more opportunities to USPIO nanoparticles for targeting tumors through the EPR effect. Xie et al. reported the USPIO formed by coating 2.0 nm iron oxide particles with thin and hydrophilic SH as mentioned above for tumor imaging (Xie, Wang, et al., 2020). The bright signals of the

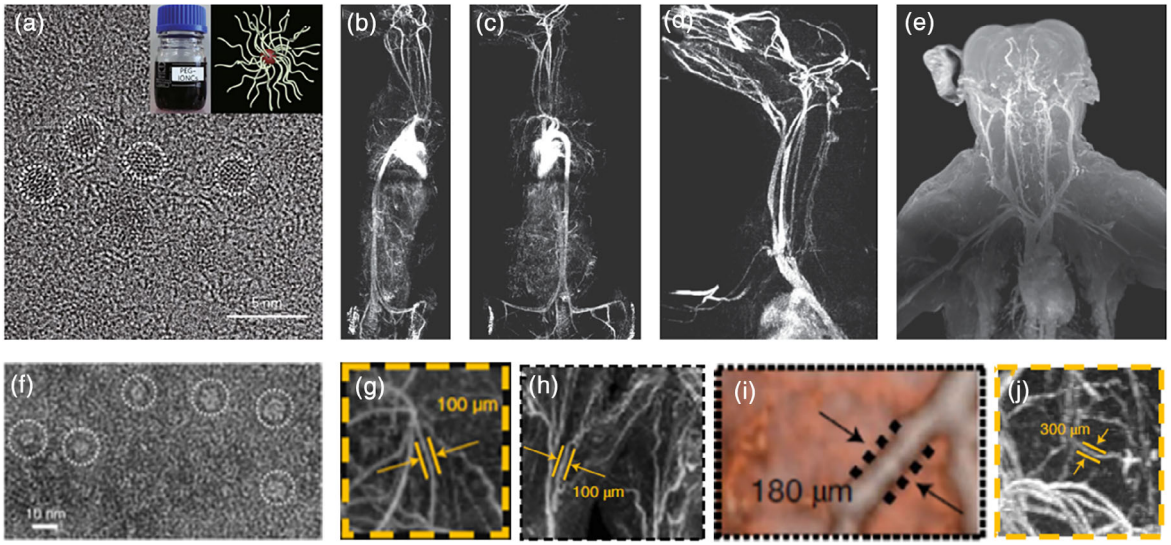

FIGURE 4 (a) High-resolution TEM image of PEGylated USPIO nanoparticles; (b–d) USPIO-enhanced arterial MRA of the whole body (b,c) and upper body (d) of a beagle dog; (e) USPIO-enhanced MRA of the upper body of a macaque (Reprinted with permission from Y. Lu et al., 2017, Copyright 2017, Springer Nature); (f) negatively stained TEM image of USPIO; (g–j) T_1-weighted MRI of brain vessels (g), peripheral vessels (h), and coronary vessels (i) of rodents and lower-extremity vessels of rabbits (j), respectively (Reprinted with permission from Shin et al., 2021, Copyright 2021, Springer Nature). MRA, magnetic resonance angiography; MRI, magnetic resonance imaging; PEG, polyethylene glycol; TEM, transmission electron microscope; USPIO, ultrasmall superparamagnetic iron oxide

tumor area reached the maxima at 70 min after the intravenous injection of the USPIO particles into mice with tumor xenografts through T_1-weighted MRI, which was explained by EPR-associated passive targeting. Zhou et al. reported zwitterion-coated 4.8 nm Gd-embedded iron oxide particles for tumor imaging through passive targeting on a subcutaneous SKOV3 ovarian cancer model (Zhou et al., 2013). After intravenous injection, the T_1 MRI signals of the tumor site increased over time, giving rise to the highest contrast between tumor and surrounding tissues at 2.0 h, as shown in Figure 5(a),(b). Gao group also reported tumor imaging studies through EPR effect (Zeng, Jing, et al., 2014). They prepared HX-PEG-coated 3.6 nm USPIO that presented high T_1/T_2 dual-modal contrast enhancement. The T_1 and T_2 MRI signals of the tumorous site increased synchronously and then decreased gradually, providing a maximum ΔR_1 of 33% and ΔR_2 of 54% at approximately 4.0 h postinjection, as shown in Figure 5(c),(d).

Although USPIO is easier to extravasate from the tumor vasculature, but the enhanced intravasation is also worth being noted. It is reported that large size nanoparticles have a significant EPR effect due to their limited intravasation of the extravasated particles back into the blood circulation, which inspires researchers to explore a feasible way to enhance the EPR effect of USPIO nanoparticles (Cabral et al., 2011). As mentioned before, the relaxation time and MR imaging contrast behavior can be tuned by the aggregation states of USPIO nanoparticles, for example, the clustering of USPIO nanoparticles can significantly decrease the T_1 effect while increase the T_2 effect (D. Ma et al., 2020). Thus, the following strategy was proposed, that is, delivering the assembled USPIO nanoparticles into tumors to take the advantage of stronger EPR effect of larger particles, and then disassembling them under the stimulation of tumor microenvironment to recover the strong T_1 effect of USPIO. As the assembled USPIO particles taken up by normal tissue present strong T_2 effect, while the disassembled particles within tumorous site present strong T_1 effect, the contrast between the tumorous site and the surrounding tissues is thus improved. This strategy has been demonstrated to be effective for detecting small hepatocellular carcinoma (HCC) (Figure 6(a)) (J. Lu et al., 2018). In this study, the anchor DNA-modified USPIO nanoparticles were cross-linked by pH-responsive i-motif DNAs to generate particle clusters that were disassembled into individual USPIO nanoparticles again in acidic tumor environment, which gives rise to improved contrast between the normal liver and the HCC tumor at 2.0 h postinjection, significantly better than the non-responsive USPIO probes, as shown in Figure 6(b).

In such an "one-directional" approach, the intravasation of large particle clusters from tumor tissue interstitial to blood vessels is expected to be slow. However, the formation of large particle clusters will shorten the blood circulation time, which makes this approach specifically suitable for liver cancer diagnosis. Regarding the diagnosis of other tumors, a "bidirectional" combining enhanced extravasation and reduced intravasation was proposed for improving the

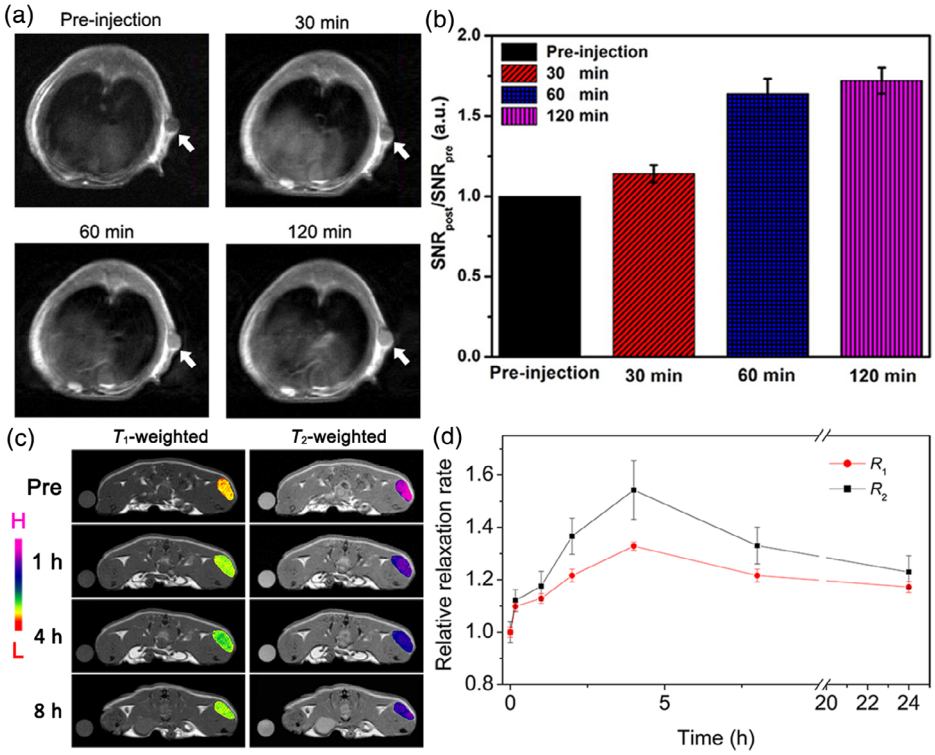

FIGURE 5 (a) T_1-weighted MRI and (b) quantificational analysis of the temporal SNR of tumors after intravenous injection of 4.8 nm Gd-embedded ZDS-coated USPIO nanoparticles (Reprinted with permission from Zhou et al., 2013, Copyright 2013, American Chemical Society); (c) T_1-weighted and T_2-weighted MRI and (d) the temporal evolution of R_1 and R_2 values of tumors after intravenous injection of HX-PEG-coated 3.6 nm USPIO nanoparticles (Reprinted with permission from Zeng, Jing, et al., 2014, Copyright 2014, Wiley). Gd, gadolinium; HX, hydroxamate; MRI, magnetic resonance imaging; PEG, polyethylene glycol; SNR, signal-to-noise ratio; USPIO, ultrasmall superparamagnetic iron oxide; ZDS, zwitterionic dopamine sulfonate

EPR effect. Specifically, USPIO nanoparticles in dispersive state are delivered and then self-assembled into particle aggregates within tumors to suppress their reentry into the blood circulation (Zhou et al., 2017). Wang et al. compared SPIO particles of 10 and 20 nm with 3.5 nm USPIO particles for 4 T1 tumor imaging (L. Wang, Huang, et al., 2017). They found that USPIO particles coated by oligosaccharide exhibited a deeper tumor penetration and greater tumor accumulation because of the enhanced tumor passive targeting ability gained through self-assembly. As shown in Figure 6(c)–(e), the 3.5 nm USPIO particles can reach the area as far as 60–80 μm away from the vascular wall, but this distance is only of 10 μm for the 20 nm SPIO nanoparticles. The self-assembling behavior of USPIO particles in the tumors was explained by the gradual protonation of carboxyl groups on the particle surface induced by acidic tumor microenvironment. As expected, a switch from the bright T_1 contrast at 60 min postinjection to the dark T_2 contrast of the tumor site at 24 h later was observed after intravenous injection of USPIO (Figure 6(f)). Gao group also developed a T_1 to T_2 conversion imaging probe for MRI of small intracranial tumor (2.4 mm × 1.6 mm) (Figure 7(a)) (Zhang et al., 2021). They modified the surface of USPIO with angiopep-2 peptide for crossing the blood–brain barrier to deliver the USPIO particles to target the brain glioma. Simultaneously, they introduced maleimide surface residues that can react with thiol group generated by reducing the disulfide bond embedded in the peptide sequence with GSH. With such a responsive design, the monodisperse USPIO particles can form agglomerate in the presence of GSH that is highly excreted in tumor microenvironment, which gives rise to T_1/T_2 interlocked variations of T_1 and T_2 signals (Figure 7(b), (c)). As shown in Figure 7(d), after intravenous injection of the GSH-responsive nanoprobe, the T_1 signal in the tumor area reached the maximum intensity at 3.0 h and then declined, but still kept identifiable at 9.0 h. In difference, the T_2 signal began to present a low part at 1.0 h and reached a plateau between 3.0 and 5.0 h, and then increased significantly again at 7.0 h postinjection. In comparison with the nonresponsive nanoprobe, the GSH-responsive nanoprobe exhibited prolonged contrast enhancement time and interlocked signal variations, which is greatly helpful for excluding false diagnosis.

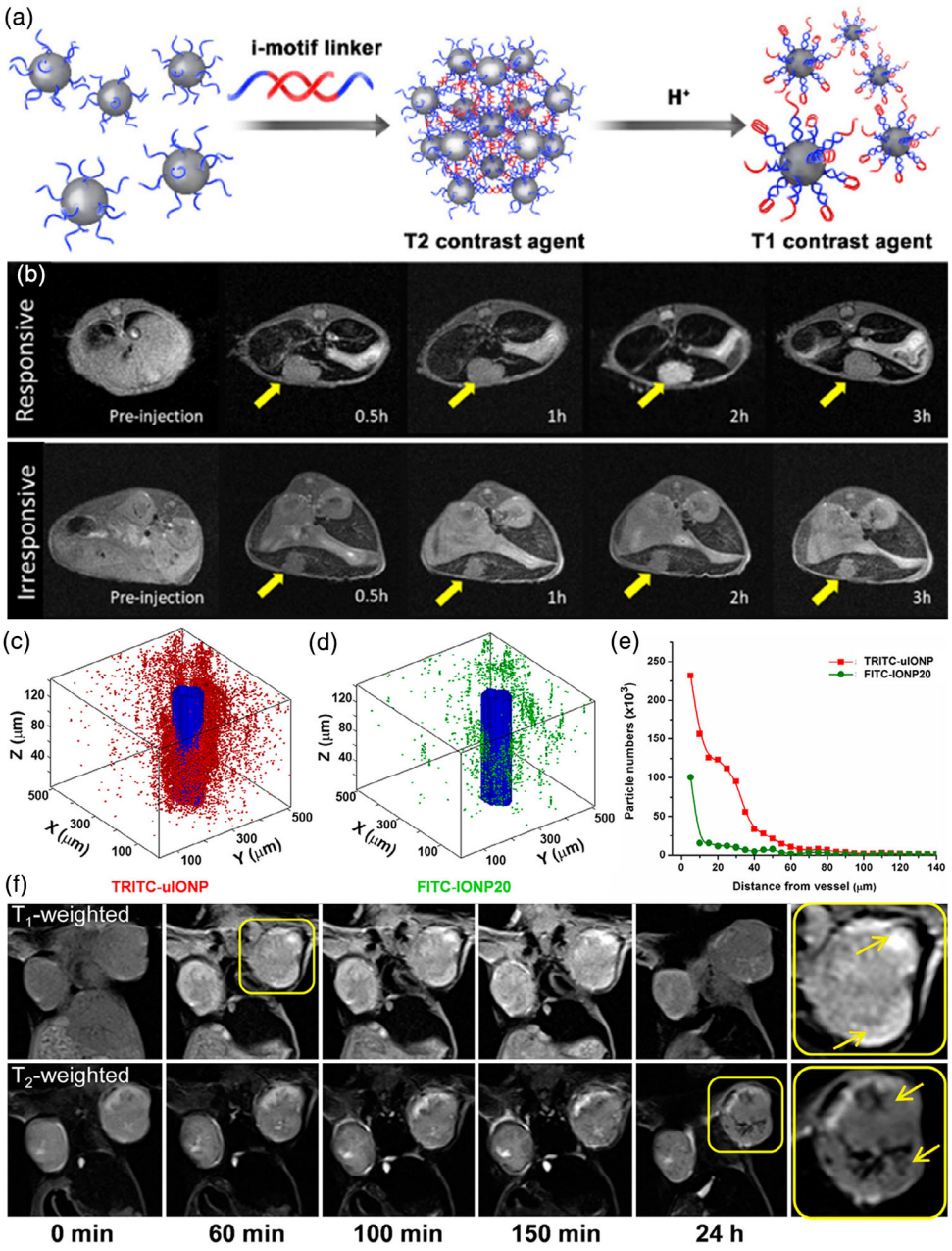

FIGURE 6 (a) Illustration of the mechanism of HCC imaging using pH-responsive USPIO nanoparticles for T_1/T_2 MRI; (b) in vivo T_1-weighted MRI of acid responsive USPIO-based assembly (top) and nonresponsive USPIO-based assembly (bottom) (Reprinted with permission from J. Lu et al., 2018, Copyright 2018, American Chemical Society); (c,d) three-dimensional model reconstruction to show the distribution of oligosaccharide-coated 3.5 nm USPIO nanoparticles and 20 nm SPIO nanoparticles in tumor; and (e) the analysis on the distance between nanoparticles and blood vessels; (f) in vivo MRI of tumors with the aid of USPIO nanoparticles as contrast agents (Reprinted with permission from L. Wang, Huang, et al., 2017, Copyright 2017, American Chemical Society). HCC, hepatocellular carcinoma; MRI, magnetic resonance imaging; USPIO, ultrasmall superparamagnetic iron oxide

Furthermore, in order to improve tumor targeting ability of the contrast particles, conjugating functional tumor-specific ligands, for example, hyaluronic acid, folic acid, antibodies, aptamers, and peptides, to the surface of USPIO nanoparticles has become one of the main strategies, to realize the so-called active targeting (Darguzyte et al., 2020; Duan et al., 2019; Z. Gao et al., 2017; Luo et al., 2015; Wu et al., 2018; Yin et al., 2019). For example, based on the specific interaction with integrin $\alpha_v\beta_3$ overexpressed on the angiogenic tumor vessels, the arginine-glycine-aspartic (RGD) peptide is often adopted to improve the accumulation of USPIO nanoparticles in the tumor site (S. Deng et al., 2015; Sun et al., 2018; Xue et al., 2015; J. Yang et al., 2015). Bai et al. reported a RGD-modified USPIO (USPIO-RGD) probe

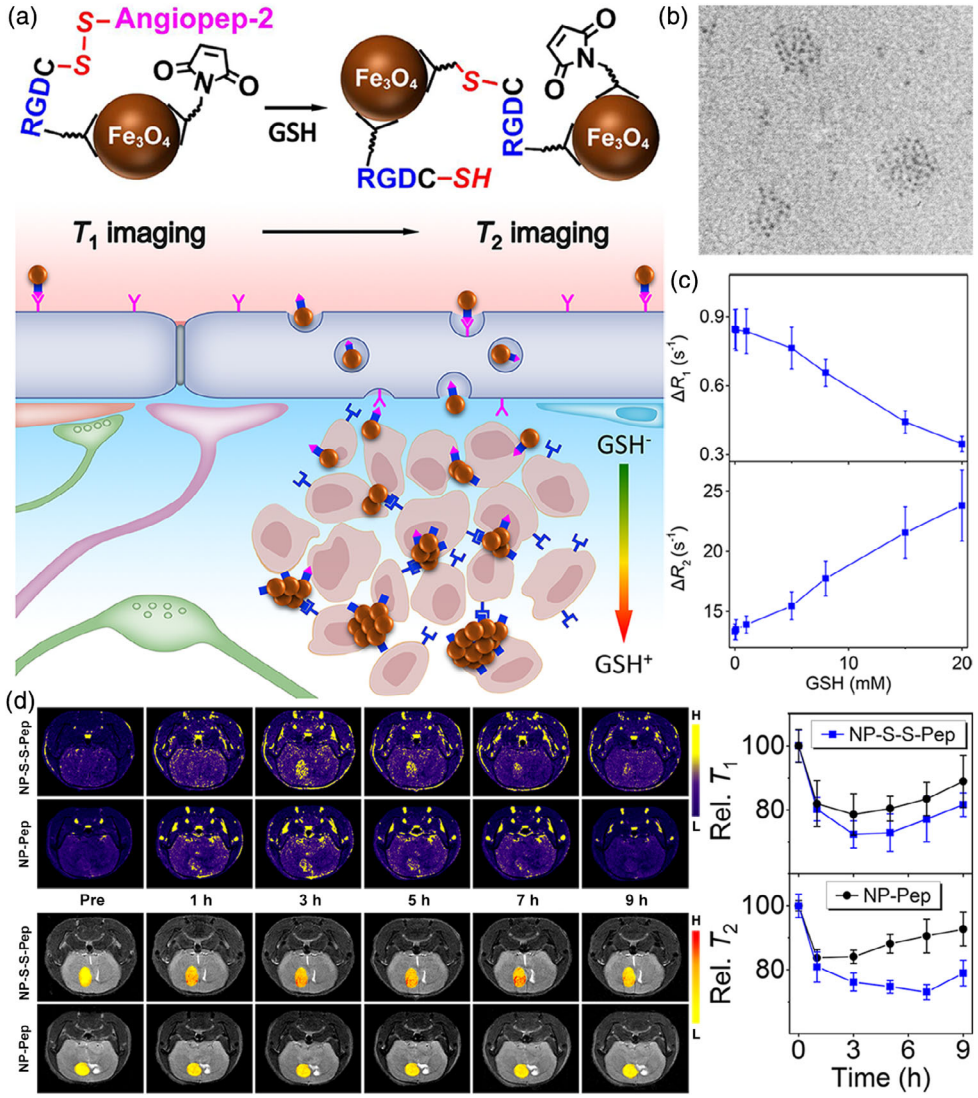

FIGURE 7 (a) Schematic diagram of a responsive nanoprobe based on GSH-induced aggregation of USPIO nanoparticles for T_1/T_2-weighted MRI of intracranial tumors; (b) TEM image of USPIO particle clusters formed in the presence of GSH; (c) GSH concentration dependent ΔR_1 and ΔR_2 of GSH-responsive USPIO nanoparticles in vitro; (d) T_1-weighted (top) and T_2-weighted (bottom) MRI of brain glioma acquired at different time points after the intravenous injections of GSH-responsive and nonresponsive probes, respectively, together with the quantified T_1 and T_2 signal placed right-hand side (Reprinted with permission from Zhang et al., 2021, Copyright 2021, Wiley). GSH, glutathione; MRI, magnetic resonance imaging; TEM, transmission electron microscope; USPIO, ultrasmall superparamagnetic iron oxide

and the following in vivo imaging studies clearly showed that the integrin $\alpha_v\beta_3$-specific USPIO-RGD gave rise to effectively improved T_1 contrast in comparison to its mother particle, which was caused by the improved accumulation of USPIO-RGD as demonstrated through Prussian blue and immunohistochemical staining (Bai et al., 2018). However, targeting ligands may also bind to the cells of nontarget site, decreasing the bioavailability of the nanoprobe. To alleviate this problem, Shen et al. intelligently modified acid-sensitive PEG on the poly(acrylic acid) (PAA) stabilized 3.6 nm USPIO to hide RGD residues within the surface coating layer in the neutral bloodstream, while in the acidic tumor environment the PEG segment was detached to expose the RGD moieties for firmly binding the USPIO with the tumor cells (Shen, Chen, et al., 2017). In T_1-weighted MRI, the above smart nanoprobes exhibited a tumor ΔSNR up to 203.4% at 12 h post-injection, much higher than those achieved by the PAA-stabilized USPIO and Gd-DTPA controls. In addition, it is worth mentioning that the designed nanoprobes enabled much higher ΔSNR in tumor than that in liver and in spleen, implying their outstanding efficacy for tumor targeting. To sum up, USPIO enables versatile approaches including EPR-mediated passive targeting and tumor-specific ligands-directed active targeting for tumor diagnosis owing to its unique properties associated with the small particle size, aggregation-dependent relaxation properties, and high specific surface area.

3.3 | Atherosclerosis imaging

Atherosclerosis is a kind of chronic inflammation of arterial wall caused by the accumulation of lipid, resulting in arterial narrowing and thrombosis (J. Chen et al., 2021; Evans et al., 2020). It is the primary cause of many lethal cardiovascular diseases, such as acute myocardial infarction and stroke (R. Qiao et al., 2020). T_1-weighted MRI is especially suitable for the imaging of vascular thrombosis, because the thrombus presents bright signal in the image, while the surrounding tissue and blood generate dark signals, giving rise to a large contrast (Ta et al., 2017). USPIO nanoparticles

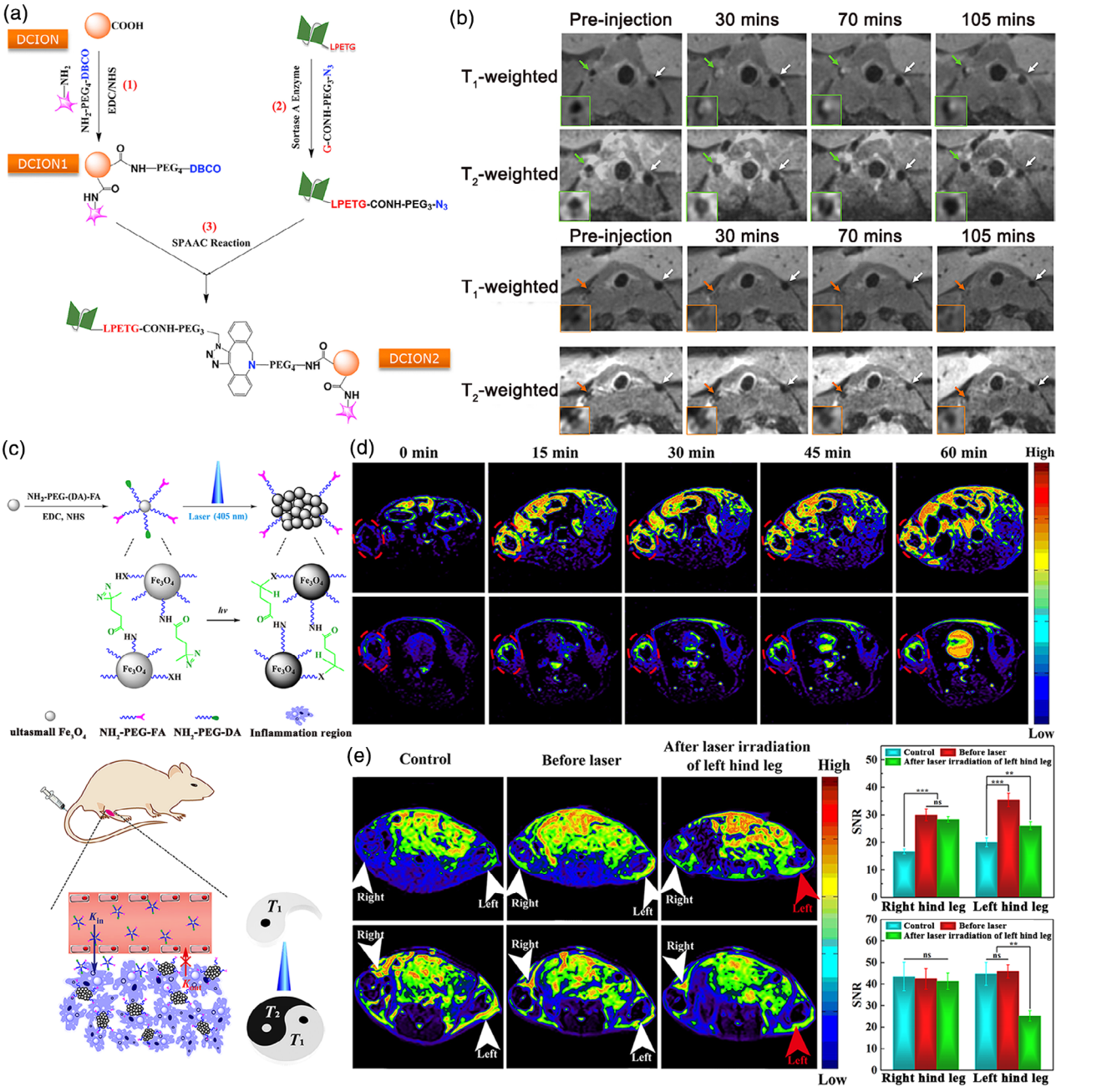

FIGURE 8 (a) Schematic illustration of the preparation of USPIO-scFv conjugates; (b) T_1-weighted and T_2-weighted MRI of carotid arteries with USPIO-scFv nanoprobe (top) and the mother USPIO as control (bottom) (Reprinted with permission from Ta et al., 2017, Copyright 2017, Elsevier); (c) schematic illustration of T_1/T_2 MRI for inflammation based on the light-triggered USPIO nanoprobes; (d) T_1-weighted MRI of normal arthritis (top) and folate inhibited arthritis models (bottom); (e) T_1-weighted (top) and T_2-weighted (bottom) MRI, and the corresponding quantified data of arthritis area acquired before and after laser irradiation (Reprinted with permission from X. Li, Lu, et al., 2019, Copyright 2019, Wiley). MRI, magnetic resonance imaging; USPIO, ultrasmall superparamagnetic iron oxide

possess a long blood circulation time and are able to enter the plaques through leaky endothelium. Macrophages are abundant in atherosclerotic plaques and can effectively take up USPIO to enhance T_1 MRI signal, which is very beneficial for atherosclerosis imaging (Y. Li, Pan, et al., 2019; C. L. Liu et al., 2014; Mo et al., 2020; Smits et al., 2017).

Pellico et al. studied the potential of MRI for atherosclerosis diagnosis through ex vivo analysis of aortas from apolipoprotein E-deficient ($ApoE^{-/-}$) mice by injecting 2.8 nm ^{68}Ga-doped USPIO with a citrate coating (Pellico et al., 2019). The hyperintense areas of the lesion were clearly observed in both the axial and three-dimensional view of the aorta, indicating the accumulation of nanoparticles in the aorta. In an attempt to obtain highly sensitive and precise diagnostic information, Ta et al. developed the poly(methacrylic acid) stabilized 3.3 nm USPIO nanoparticles for targeted T_1/T_2-weighted MRI of atherothrombosis (Figure 8(a)) (Ta et al., 2017). The USPIO was modified with single-chain antibodies (scFv) to target the activated platelets that were a key player of atherosclerosis and thrombosis. The in vitro experiments proved that the USPIO-scFv probe has strong binding affinity to human thrombus. Further in vivo imaging on the mouse carotid arterial thrombus models demonstrated that USPIO-scFv induced apparent signal enhancement in both T_1-weighted MRI and T_2-weighted MRI of thrombus area, while the non-targeted USPIO produced negligible signal changes, as shown in Figure 8(b).

3.4 | Inflammation imaging

Tissue inflammation is a common pathological process in the clinic. Accurate and clear imaging of inflammatory sites is helpful for evaluating the severity of disease and monitoring the effect of anti-inflammatory treatment. Macrophage and monocyte infiltration are important markers for tissue inflammation and play a central role in the pathogenesis of inflammatory diseases, for example, chronic liver diseases and obesity-related inflammation (Khaled et al., 2019). As inflammatory macrophages have a strong phagocytic ability and can effectively take up nanoparticle-based contrast agents, nano-contrast agents are suitable for MRI of inflammatory macrophages. The long circulation time increases the probability for USPIO nanoparticles to enter into the lymphatic system and be taken up by macrophages in lymph nodes or peripheral tissues, making USPIO appropriate for detecting macrophages under a number of pathological inflammatory conditions (Khan et al., 2019).

Simon et al. compared the diagnostic performance of carboxydextran-coated 3.0 nm USPIO with that of Gd-DTPA for monoarthritis through T_1-weighted MRI (Simon et al., 2006). Owing to the much longer blood half-life of 6.0 h for USPIO contrasting to 20 min for Gd-DTPA, USPIO provided a long-term T_1 enhancement of 40–120 min for arthritis, while it was only of 2.0 min for Gd-DTPA. In addition, USPIO provided a more significant T_1 contrast between arthritic areas and normal joints due to their less accumulation in normal joints than Gd-DTPA, which encourages further investigations on USPIO-based MRI for inflammation diagnosis. To accurately diagnose the inflammation area, Li et al. developed a dynamic T_1/T_2-weighted MRI for inflammatory arthritis in vivo based on a light-addressable assembly of citric acid-stabilized USPIO (X. Li, Lu, et al., 2019). As shown in Figure 8(c), they modified USPIO with a light-addressable unit diazirine and arthritis-specific ligand folic acid via a PEG linker to realize very unique light-responsive aggregation for targeting arthritis-related macrophages. As shown in Figure 8(d), the USPIO-based nanoprobe showed an excellent T_1 MRI performance for inflammatory area. In addition, under the excitation of 405 nm laser, USPIO nanoprobes were capable of forming particles clusters with high r_2 relaxivity. The formation of the particle clusters is expected to suppress the intravasation of particle probes back to the blood circulation from the lesion region. Therefore, the smart-designed light-sensitive USPIO nanoprobes exhibit flexible and controllable dynamic T_1/T_2 MRI for arthritis, as shown in Figure 8(e), which is effective for improving the diagnosis precision.

4 | CONCLUSION

With lots of unique characteristics, USPIO nanoparticles become superior to the traditional counterparts, for example, GBCAs and SPIO nanoparticles, and will surely open an avenue towards advanced enhanced MRI and make the accurate diagnosis of diseases step forward into a new era. First of all, USPIO nanoparticles possess low magnetization caused by the spin canting effect that effectively shortens the T_1 relaxation time of protons, which is beneficial for T_1 enhancement. Besides, USPIO nanoparticles show excellent imaging performance because the appropriate size and surface modification enable the long-term blood circulation favorable for steady-state imaging and high-resolution imaging. The renal clearance capacity of USPIO nanoparticles is also promoted to reduce the potential risk of long-term iron overload. Moreover, USPIO nanoparticles can be used to construct stimulus responsive nanoprobes via assembly/

disassembly to achieve flexible conversion between T_2- and T_1-weighted MRI modalities. Taking advantage of the specific stimulus response, USPIO nanoparticles can target the region of interest in an EPR-mediated manner, which in return improves the accuracy of MRI diagnosis. In addition, featured by large specific surface area and high loading capacity, USPIO nanoparticles are conducive to be facially modified with targeting ligands to build a smart molecular imaging probe for precise diagnosis of various diseases, especially tumors. Despite USPIO nanoparticles have shown enormous potential as the next generation MRI contrast agents, there remain great challenges which require more efforts in the future to accelerate their translation into clinical applications, specifically:

1. Large-scale synthesis of uniform and biocompatible USPIO nanoparticles remains a huge hurdle to overcome. Small batch production of USPIO nanoparticles in the laboratory is sufficient for scientific research, but it hardly meets the requirements for safety assessment prior to the clinical transformation. Developing massive production techniques for USPIO nanoparticles is essentially required for their further clinical translation.
2. Obtaining USPIO nanoparticles with higher relaxivity is very important for accurate and high-resolution MRI. There are many factors affecting the relaxivity, for example, size, crystalline nature, surface ligand modification, surface charge, and so on. Their impacts on the relaxivity of USPIO nanoparticles are still waiting for in-depth studies.
3. More specific scanning sequence and parameters for USPIO nanoparticles are also waiting for further optimizations. The relaxation properties of USPIO nanoparticles are quite different from those of classic GBCAs. It is not always possible to obtain the optimum results with the common sequence parameters developed for GBCAs. Therefore, it is imperative to develop sequence parameters for USPIO nanoparticles.
4. Further rigorous and standardized protocols need to be developed for reasonably assessing the biosafety of USPIO nanoparticles. There are great demands to develop reasonable methods for accurately revealing the pharmacokinetics, pharmacodynamics, in vivo fate of USPIO nanoparticles, for example, biodistribution, biotransformation, bioavailability, and so on. But there is still a lack of a comprehensive understanding on the interactions of USPIO nanoparticles with organs and tissues and the following long-term biological effects after intravenous delivery.
5. The long blood circulation time and efficient renal clearance remain the two key parameters to be optimized before the return of the advanced USPIO into the clinical applications. The properly long retention time in the body is helpful for increasing enrichment of USPIO nanoparticles in lesion regions to improve SNR and imaging contrast, while effective renal clearance helps lower the potential risk of USPIO nanoparticles in vivo. How to reasonably balance the retention time and clearance time of USPIO is worthy of careful studies.

In summary, the recently developed advanced USPIO nanoparticles hold great promise for clinical applications as they are apparently in many aspects superior to conventional Gd/Mn-based T_1 and SPIO-based T_2 contrast agents. Although the clinical translation of given inorganic nanoparticles for in vivo applications is far more complex than conventional drugs as mentioned above, the return of USPIO into clinical applications will be seen soon.

ACKNOWLEDGMENTS

The authors thank the financial support from the National Key Research and Development Program of China (2018YFA0208800), the National Natural Science Foundation of China (81720108024), the Nature Science Foundation of Jiangsu Higher Education Institutions of China (20KJA150006), the Natural Science Foundation of Jiangsu Province (BK20191418), the Suzhou Key Industry Technology Innovation Projects (SYG202036), and the Priority Academic Program Development of Jiangsu Higher Education Institutions (PAPD).

CONFLICT OF INTEREST

The authors have declared no conflicts of interest for this article.

AUTHOR CONTRIBUTIONS

Can Chen: Writing - original draft. **Jianxian Ge:** Writing - original draft. **Yun Gao:** Writing - original draft. **Lei Chen:** Writing - original draft. **Jiabin Cui:** Writing-review & editing. **Jianfeng Zeng:** Supervision; writing-review & editing. **Mingyuan Gao:** Funding acquisition; supervision; writing-review & editing.

DATA AVAILABILITY STATEMENT

Data sharing is not applicable to this article as no new data were created or analyzed in this study.

ORCID

Mingyuan Gao https://orcid.org/0000-0002-7360-3684

RELATED WIREs ARTICLES

Superparamagnetic iron oxide nanoparticles for MRI: contrast media pharmaceutical company R&D perspective
Paramagnetic inorganic nanoparticles as T1 MRI contrast agents
Ultra-small superparamagnetic iron oxides for metastatic lymph node detection: back on the block
Monodisperse magnetic nanoparticles for biodetection, imaging, and drug delivery: a versatile and evolving technology

REFERENCES

Abbas, H., Broche, L. M., Ezdoglian, A., Li, D., Yuecel, R., James Ross, P., Cheyne, L., Wilson, H. M., Lurie, D. J., & Dawson, D. K. (2020). Fast field-cycling magnetic resonance detection of intracellular ultra-small iron oxide particles *in vitro*: Proof-of-concept. *Journal of Magnetic Resonance*, *313*, 106722. https://doi.org/10.1016/j.jmr.2020.106722

Alam, S. R., Stirrat, C., Richards, J., Mirsadraee, S., Semple, S. I. K., Tse, G., Henriksen, P., & Newby, D. E. (2015). Vascular and plaque imaging with ultrasmall superparamagnetic particles of iron oxide. *Journal of Cardiovascular Magnetic Resonance*, *17*, 83. https://doi.org/10.1186/s12968-015-0183-4

Bai, C., Jia, Z., Song, L., Zhang, W., Chen, Y., Zang, F., Ma, M., Gu, N., & Zhang, Y. (2018). Time-dependent T_1–T_2 switchable magnetic resonance imaging realized by c(RGDyK) modified ultrasmall Fe_3O_4 nanoprobes. *Advanced Functional Materials*, *28*(32), 1802281. https://doi.org/10.1002/adfm.201802281

Bao, Y., Sherwood, J. A., & Sun, Z. (2018). Magnetic iron oxide nanoparticles as T_1 contrast agents for magnetic resonance imaging. *Journal of Materials Chemistry C*, *6*(6), 1280–1290. https://doi.org/10.1039/c7tc05854c

Bietenbeck, M., Florian, A., Sechtem, U., & Yilmaz, A. (2015). The diagnostic value of iron oxide nanoparticles for imaging of myocardial inflammation - quo vadis? *Journal of Cardiovascular Magnetic Resonance*, *17*, 54. https://doi.org/10.1186/s12968-015-0165-6

Cabral, H., Matsumoto, Y., Mizuno, K., Chen, Q., Murakami, M., Kimura, M., Terada, Y., Kano, M. R., Miyazono, K., Uesaka, M., Nishiyama, N., & Kataoka, K. (2011). Accumulation of sub-100 nm polymeric micelles in poorly permeable tumours depends on size. *Nature Nanotechnology*, *6*(12), 815–823. https://doi.org/10.1038/nnano.2011.166

Cai, X., Zhu, Q., Zeng, Y., Zeng, Q., Chen, X., & Zhan, Y. (2019). Manganese oxide nanoparticles as MRI contrast agents in tumor multimodal imaging and therapy. *International Journal of Nanomedicine*, *14*, 8321–8344. https://doi.org/10.2147/IJN.S218085

Cao, Y., He, Y., Mao, Z., Kuang, Y., Liu, M., Zhang, Y., & Pei, R. (2020). Synergistic regulation of longitudinal and transverse relaxivity of extremely small iron oxide nanoparticles (ESIONPs) using pH-responsive nanoassemblies. *Nanoscale*, *12*(33), 17502–17516. https://doi.org/10.1039/d0nr04201c

Cao, Y., Mao, Z., He, Y., Kuang, Y., Liu, M., Zhou, Y., Zhang, Y., & Pei, R. (2020). Extremely small iron oxide nanoparticle-encapsulated nanogels as a glutathione-responsive T_1 contrast agent for tumor-targeted magnetic resonance imaging. *ACS Applied Materials & Interfaces*, *12*(24), 26973–26981. https://doi.org/10.1021/acsami.0c07288

Caspani, S., Magalhaes, R., Araujo, J. P., & Sousa, C. T. (2020). Magnetic nanomaterials as contrast agents for MRI. *Materials*, *13*(11), 2586. https://doi.org/10.3390/ma13112586

Chen, J., Zhang, X., Millican, R., Sherwood, J., Martin, S., Jo, H., Yoon, Y. S., Brott, B. C., & Jun, H. W. (2021). Recent advances in nanomaterials for therapy and diagnosis for atherosclerosis. *Advanced Drug Delivery Reviews*, *170*, 142–199. https://doi.org/10.1016/j.addr.2021.01.005

Chen, R., Ling, D., Zhao, L., Wang, S., Liu, Y., Bai, R., Baik, S., Zhao, Y., Chen, C., & Hyeon, T. (2015). Parallel comparative studies on mouse toxicity of oxide nanoparticle- and gadolinium-based T_1 MRI contrast agents. *ACS Nano*, *9*(12), 12425–12435. https://doi.org/10.1021/acsnano.5b05783

Choi, S. H., Liu, W., Misra, P., Tanaka, E., Zimmer, J. P., Itty Ipe, B., Bawendi, M. G., & Frangioni, J. V. (2007). Renal clearance of quantum dots. *Nature Biotechnology*, *25*(10), 1165–1170. https://doi.org/10.1038/nbt1340

Daldrup-Link, H. E. (2017). Ten things you might not know about iron oxide nanoparticles. *Radiology*, *284*(3), 616–629. https://doi.org/10.1148/radiol.2017162759

Darguzyte, M., Drude, N., Lammers, T., & Kiessling, F. (2020). Riboflavin-targeted drug delivery. *Cancers*, *12*(2), 295. https://doi.org/10.3390/cancers12020295

Deng, L. H., Jiang, H., Lu, F. L., Wang, H. W., Pu, Y., Wu, C. Q., Tang, H. J., Xu, Y., Chen, T. W., Zhu, J., Shen, C. Y., & Zhang, X. M. (2021). Size and PEG length-controlled PEGylated monocrystalline superparamagnetic iron oxide nanocomposite for MRI contrast agent. *International Journal of Nanomedicine*, *16*, 201–211. https://doi.org/10.2147/IJN.S271461

Deng, S., Zhang, W., Zhang, B., Hong, R., Chen, Y., Dong, J., Chen, Y., Chen, Z., & Wu, Y. (2015). Radiolabeled cyclic arginine-glycine-aspartic (RGD)conjugated iron oxide nanoparticles as single-photon emission computed tomography (SPECT) and magnetic resonance imaging (MRI) dual-modality agents for imaging of breast cancer. *Journal of Nanoparticle Research*, *17*, 19. https://doi.org/10.1007/s11051-014-2845-9

Du, C., Liu, X., Hu, H., Li, H., Yu, L., Geng, D., Chen, Y., & Zhang, J. (2020). Dual-targeting and excretable ultrasmall SPIONs for T_1-weighted positive MR imaging of intracranial glioblastoma cells by targeting the lipoprotein receptor-related protein. *Journal of Materials Chemistry B*, *8*(11), 2296–2306. https://doi.org/10.1039/c9tb02391g

Duan, Y., Hu, D., Guo, B., Shi, Q., Wu, M., Xu, S., Kenry, Liu, X., Jiang, J., Sheng, Z., Zheng, H., & Liu, B. (2019). Nanostructural control enables optimized photoacoustic–fluorescence–magnetic resonance multimodal imaging and photothermal therapy of brain tumor. *Advanced Functional Materials*, *30*(1), 1907077. https://doi.org/10.1002/adfm.201907077

Duyn, J. H., Gelderen, P. V., Li, T.-Q., Zwart, J. A. D., Koretsky, A. P., & Fukunaga, M. (2007). High-field MRI of brain cortical substructure based on signal phase. *Proceedings of the National Academy of Sciences of the United States of America*, *104*(28), 11796–11801. https://doi.org/10.1073/pnas.0610821104

Eamegdool, S. S., Weible, M. W., II, Pham, B. T. T., Hawkett, B. S., Grieve, S. M., & Chan-ling, T. (2014). Ultrasmall superparamagnetic iron oxide nanoparticle prelabelling of human neural precursor cells. *Biomaterials*, *35*(21), 5549–5564. https://doi.org/10.1016/j.biomaterials.2014.03.061

Ehlerding, E. B., Chen, F., & Cai, W. (2016). Biodegradable and renal clearable inorganic nanoparticles. *Advanced Science*, *3*(2), 1500223. https://doi.org/10.1002/advs.201500223

Evans, R. J., Lavin, B., Phinikaridou, A., Chooi, K. Y., Mohri, Z., Wong, E., Boyle, J. J., Krams, R., Botnar, R., & Long, N. J. (2020). Targeted molecular iron oxide contrast agents for imaging atherosclerotic plaque. *Nano*, *4*(4), 184–194. https://doi.org/10.7150/ntno.44712

Feng, J., Chen, C., Zhao, J., Hao, F., Bhakoo, K., & Tang, H. (2010). NMR-based metabonomic analyses of the effects of ultrasmall superparamagnetic particles of iron oxide (USPIO) on macrophage metabolism. *Journal of Nanoparticle Research*, *13*(5), 2049–2062. https://doi.org/10.1007/s11051-010-9959-5

Gao, Z., Hou, Y., Zeng, J., Chen, L., Liu, C., Yang, W., & Gao, M. (2017). Tumor microenvironment-triggered aggregation of antiphagocytosis ^{99m}Tc-labeled Fe_3O_4 nanoprobes for enhanced tumor imaging *in vivo*. *Advanced Materials*, *29*(24), 1701095. https://doi.org/10.1002/adma.201701095

Gao, Z. Y., Ma, T. C., Zhao, E. Y., Docter, D., Yang, W. S., Stauber, R. H., & Gao, M. Y. (2015). Small is smarter: Nano MRI contrast agents—Advantages and recent achievements. *Small*, *12*(5), 556–576. https://doi.org/10.1002/smll.201502309

Garcia-Fernandez, J., Turiel, D., Bettmer, J., Jakubowski, N., Panne, U., Rivas García, L., Llopis, J., Sánchez González, C., & Montes-Bayón, M. (2020). *In vitro* and *in situ* experiments to evaluate the biodistribution and cellular toxicity of ultrasmall iron oxide nanoparticles potentially used as oral iron supplements. *Nanotoxicology*, *14*(3), 388–403. https://doi.org/10.1080/17435390.2019.1710613

Gharehaghaji, N., Nazarpoor, M., & Saharkhiz, H. (2015). Effect of flip angle on the correlation between signal intensity and different concentrations of iron oxide nanoparticles using T_1-weighted turbo-FLASH inversion recovery sequence. *Iranian Journal of Radiology*, *12*(2), 22887. https://doi.org/10.5812/iranjradiol.22887

Hao, X., Xu, B., Chen, H., Wang, X., Zhang, J., Guo, R., Shi, X., & Cao, X. (2019). Stem cell-mediated delivery of nanogels loaded with ultrasmall iron oxide nanoparticles for enhanced tumor MR imaging. *Nanoscale*, *11*(11), 4904–4910. https://doi.org/10.1039/c8nr10490e

He, C., Jiang, S., Yao, H., Zhang, L., Yang, C., Zhan, D., Lin, G., Zeng, Y., Xia, Y., Lin, Z., Liu, G., & Lin, Y. (2018). Endoplasmic reticulum stress mediates inflammatory response triggered by ultra-small superparamagnetic iron oxide nanoparticles in hepatocytes. *Nanotoxicology*, *12*(10), 1198–1214. https://doi.org/10.1080/17435390.2018.1530388

Hu, F., Jia, Q., Li, Y., & Gao, M. (2011). Facile synthesis of ultrasmall PEGylated iron oxide nanoparticles for dual-contrast T_1- and T_2-weighted magnetic resonance imaging. *Nanotechnology*, *22*(24), 245604. https://doi.org/10.1088/0957-4484/22/24/245604

Huang, G., Li, H., Chen, J., Zhao, Z., Yang, L., Chi, X., Chen, Z., Wang, X., & Gao, J. (2014). Tunable T_1 and T_2 contrast abilities of manganese-engineered iron oxide nanoparticles through size control. *Nanoscale*, *6*(17), 10404–10412. https://doi.org/10.1039/c4nr02680b

Jeon, M., Halbert, M. V., Stephen, Z. R., & Zhang, M. (2020). Iron oxide nanoparticles as T_1 contrast agents for magnetic resonance imaging: Fundamentals, challenges, applications, and prospectives. *Advanced Materials*, *33*, 1906539. https://doi.org/10.1002/adma.201906539

Jia, L., Li, X., Liu, H., Xia, J., Shi, X., & Shen, M. (2021). Ultrasound-enhanced precision tumor theranostics using cell membrane-coated and pH-responsive nanoclusters assembled from ultrasmall iron oxide nanoparticles. *Nano Today*, *36*, 101022. https://doi.org/10.1016/j.nantod.2020.101022

Jin, R., Lin, B., Li, D., & Ai, H. (2014). Superparamagnetic iron oxide nanoparticles for MR imaging and therapy: Design considerations and clinical applications. *Current Opinion in Pharmacology*, *18*, 18–27. https://doi.org/10.1016/j.coph.2014.08.002

Kamer, K. J., Sancak, Y., Fomina, Y., Meisel, J. D., Chaudhuri, D., Grabarek, Z., & Mootha, V. K. (2018). MICU1 imparts the mitochondrial uniporter with the ability to discriminate between Ca^{2+} and Mn^{2+}. *Proceedings of the National Academy of Sciences of the United States of America*, *115*(34), 7960–7969. https://doi.org/10.1073/pnas.1807811115

Khaled, W., Piraquive, J., Leporq, B., Wan, J. H., Lambert, S. A., Mignet, N., Doan, B. T., Lotersztajn, S., Garteiser, P., & van Beers, B. E. (2019). *In vitro* distinction between proinflammatory and antiinflammatory macrophages with gadolinium-liposomes and ultrasmall superparamagnetic iron oxide particles at 3.0T. *Journal of Magnetic Resonance Imaging*, *49*(4), 1166–1173. https://doi.org/10.1002/jmri.26331

Khan, S., Amin, F. M., Fliedner, F. P., Christensen, C. E., Tolnai, D., Younis, S., Olinger, A. C. R., Birgens, H., Daldrup-Link, H., Kjær, A., Larsson, H. B. W., Lindberg, U., & Ashina, M. (2019). Investigating macrophage-mediated inflammation in migraine using ultrasmall superparamagnetic iron oxide-enhanced 3T magnetic resonance imaging. *Cephalalgia*, *39*(11), 1407–1420. https://doi.org/10.1177/0333102419848122

Kim, B. H., Lee, N., Kim, H., An, K., Park, Y. I., Choi, Y., Shin, K., Lee, Y., Kwon, S. G., Na, H. B., Park, J. G., Ahn, T. Y., Kim, Y. W., Moon, W. K., Choi, S. H., & Hyeon, T. (2011). Large-scale synthesis of uniform and extremely small-sized iron oxide nanoparticles for high-resolution T_1 magnetic resonance imaging contrast agents. *Journal of the American Chemical Society*, *133*(32), 12624–12631. https://doi.org/10.1021/ja203340u

Koenig, S. H., & Kellar, K. E. (1995). Theory of $1/T_1$ and $1/T_2$ NMRD profiles of solutions of magnetic nanoparticles. *Magnetic Resonance in Medicine*, *34*(2), 227–233. https://doi.org/10.1002/mrm.1910340214

Lagan, J., Naish, J. H., Simpson, K., Zi, M., Cartwright, E. J., Foden, P., Morris, J., Clark, D., Birchall, L., Caldwell, J., Trafford, A., Fortune, C., Cullen, M., Chaudhuri, N., Fildes, J., Sarma, J., Schelbert, E. B., Schmitt, M., Piper Hanley, K., & Miller, C. A. (2020). Substrate for the myocardial inflammation-heart failure hypothesis identified using novel USPIO methodology. *JACC: Cardiovasc Imaging*, *14*(2), 365–376. https://doi.org/10.1016/j.jcmg.2020.02.001

Ledda, M., Fioretti, D., Lolli, M. G., Papi, M., di Gioia, C., Carletti, R., Ciasca, G., Foglia, S., Palmieri, V., Marchese, R., Grimaldi, S., Rinaldi, M., & Lisi, A. (2020). Biocompatibility assessment of sub-5 nm silica-coated superparamagnetic iron oxide nanoparticles in human stem cells and in mice for potential application in nanomedicine. *Nanoscale*, *12*(3), 1759–1778. https://doi.org/10.1039/c9nr09683c

Lee, N., & Hyeon, T. (2012). Designed synthesis of uniformly sized iron oxide nanoparticles for efficient magnetic resonance imaging contrast agents. *Chemical Society Reviews*, *41*(7), 2575–2589. https://doi.org/10.1039/c1cs15248c

Lee, N., Kim, H., Choi, S. H., Park, M., Kim, D., Kim, H. C., Choi, Y., Lin, S., Kim, B. H., Jung, H. S., Kim, H., Park, K. S., Moon, W. K., & Hyeon, T. (2011). Magnetosome-like ferrimagnetic iron oxide nanocubes for highly sensitive MRI of single cells and transplanted pancreatic islets. *Proceedings of the National Academy of Sciences of the United States of America*, *108*(7), 2662–2667. https://doi.org/10.1073/pnas.1016409108

Lee, N., Yoo, D., Ling, D., Cho, M. H., Hyeon, T., & Cheon, J. (2015). Iron oxide based nanoparticles for multimodal imaging and magnetoresponsive therapy. *Chemical Reviews*, *115*(19), 10637–10689. https://doi.org/10.1021/acs.chemrev.5b00112

Li, F., Liang, Z., Liu, J., Sun, J., Hu, X., Zhao, M., Liu, J., Bai, R., Kim, D., Sun, X., Hyeon, T., & Ling, D. (2019). Dynamically reversible iron oxide nanoparticle assemblies for targeted amplification of T_1-weighted magnetic resonance imaging of tumors. *Nano Letters*, *19*(7), 4213–4220. https://doi.org/10.1021/acs.nanolett.8b04411

Li, J. C., Shi, X. Y., & Shen, M. W. (2014). Hydrothermal synthesis and functionalization of iron oxide nanoparticles for MR imaging applications. *Particle Particle Systems Characterization*, *31*(12), 1223–1237. https://doi.org/10.1002/ppsc.201400087

Li, X., Lu, S., Xiong, Z., Hu, Y., Ma, D., Lou, W., Peng, C., Shen, M., & Shi, X. (2019). Light-addressable nanoclusters of ultrasmall iron oxide nanoparticles for enhanced and dynamic magnetic resonance imaging of arthritis. *Advanced Science*, *6*(19), 1901800. https://doi.org/10.1002/advs.201901800

Li, Y., Pan, Y., Wu, X., Li, Y., Wang, H., Zhu, H., & Jiang, L. (2019). Dual-modality imaging of atherosclerotic plaques using ultrasmall superparamagnetic iron oxide labeled with rhodamine. *Nanomedicine*, *14*(15), 1935–1944. https://doi.org/10.2217/nnm-2019-0062

Li, Z., Yi, P. W., Sun, Q., Lei, H., Li Zhao, H., Zhu, Z. H., Smith, S. C., Lan, M. B., & Lu, G. Q. M. (2012). Ultrasmall water-soluble and biocompatible magnetic iron oxide nanoparticles as positive and negative dual contrast agents. *Advanced Functional Materials*, *22*(11), 2387–2393. https://doi.org/10.1002/adfm.201103123

Liu, C. L., Peng, Y. K., Chou, S. W., Tseng, W. H., Tseng, Y. J., Chen, H. C., Hsiao, J. K., & Chou, P. T. (2014). One-step, room-temperature synthesis of glutathione-capped iron-oxide nanoparticles and their application in *in vivo* T_1-weighted magnetic resonance imaging. *Small*, *10*(19), 3962–3969. https://doi.org/10.1002/smll.201303868

Liu, D., Zhou, Z., Wang, X., Deng, H., Sun, L., Lin, H., Kang, F., Zhang, Y., Wang, Z., Yang, W., Rao, L., Yang, K., Yu, G., du, J., Shen, Z., & Chen, X. (2020). Yolk-shell nanovesicles endow glutathione-responsive concurrent drug release and T_1 MRI activation for cancer theranostics. *Biomaterials*, *244*, 119979. https://doi.org/10.1016/j.biomaterials.2020.119979

Liu, J., Yu, M., Zhou, C., & Zheng, J. (2013). Renal clearable inorganic nanoparticles: A new frontier of bionanotechnology. *Materials Today*, *16*(12), 477–486. https://doi.org/10.1016/j.mattod.2013.11.003

Liu, S., Han, Y., Qiao, R., Zeng, J., Jia, Q., Wang, Y., & Gao, M. (2010). Investigations on the interactions between plasma proteins and magnetic iron oxide nanoparticles with different surface modifications. *The Journal of Physical Chemistry C*, *114*(49), 21270–21276. https://doi.org/10.1021/jp1086653

Lu, J., Sun, J., Li, F., Wang, J., Liu, J., Kim, D., Fan, C., Hyeon, T., & Ling, D. (2018). Highly sensitive diagnosis of small hepatocellular carcinoma using pH-responsive iron oxide nanocluster assemblies. *Journal of the American Chemical Society*, *140*(32), 10071–10074. https://doi.org/10.1021/jacs.8b04169

Lu, Y., Xu, Y. J., Zhang, G. B., Ling, D., Wang, M. Q., Zhou, Y., Wu, Y. D., Wu, T., Hackett, M. J., Hyo Kim, B., Chang, H., Kim, J., Hu, X. T., Dong, L., Lee, N., Li, F., He, J. C., Zhang, L., Wen, H. Q., … Zou, D. H. (2017). Iron oxide nanoclusters for T_1 magnetic resonance imaging of non-human primates. *Nature Biomedical Engineering*, *1*(8), 637–643. https://doi.org/10.1038/s41551-017-0116-7

Lunov, O., Syrovets, T., Büchele, B., Jiang, X., Röcker, C., Tron, K., Nienhaus, G. U., Walther, P., Mailänder, V., Landfester, K., & Simmet, T. (2010). The effect of carboxydextran-coated superparamagnetic iron oxide nanoparticles on c-Jun N-terminal kinase-mediated apoptosis in human macrophages. *Biomaterials*, *31*(19), 5063–5071. https://doi.org/10.1016/j.biomaterials.2010.03.023

Luo, Y., Gao, C., Chen, W., Zhou, K., & Xu, M. (2020). Molecular magnetic resonance imaging with contrast agents for assessment of inflammatory bowel disease: A systematic review. *Contrast Media Molecular Imaging*, *2020*, 4764985. https://doi.org/10.1155/2020/4764985

Luo, Y., Yang, J., Yan, Y., Li, J., Shen, M., Zhang, G., Mignani, S., & Shi, X. (2015). RGD-functionalized ultrasmall iron oxide nanoparticles for targeted T_1 weighted MR imaging of glioma. *Nanoscale*, *7*(34), 14538–14546. https://doi.org/10.1039/c5nr04003e

Ma, D., Chen, J., Luo, Y., Wang, H., & Shi, X. (2017). Zwitterion-coated ultrasmall iron oxide nanoparticles for enhanced T_1-weighted magnetic resonance imaging applications. *Journal of Materials Chemistry B*, *5*(35), 7267–7273. https://doi.org/10.1039/C7TB01588G

Ma, D., Shi, M., Li, X., Zhang, J., Fan, Y., Sun, K., Jiang, T., Peng, C., & Shi, X. (2020). Redox-sensitive clustered ultrasmall iron oxide nanoparticles for switchable T_2/T_1-weighted magnetic resonance imaging applications. *Bioconjugate Chemisty*, *31*(2), 352–359. https://doi.org/10.1021/acs.bioconjchem.9b00659

Ma, X., Wang, S., Hu, L., Feng, S., Wu, Z., Liu, S., Duan, S., Chen, Z., Zhou, C., & Zhao, X. (2019). Imaging characteristics of USPIO nanoparticles (<5 nm) as MR contrast agent *in vitro* and in the liver of rats. *Contrast Media & Molecular Imaging*, *2019*, 3687537. https://doi.org/10.1155/2019/3687537

Marco, M. D., Sadun, C., Port, M., Guilbert, I., Couvreur, P., & Dubernet, C. (2007). Physicochemical characterization of ultrasmall superparamagnetic iron oxide particles (USPIO) for biomedical application as MRI contrast agents. *International Journal of Nanomedicine*, *2*(4), 609–622. https://doi.org/10.2147/nano.2007.2.1.117

McDonald, R. J., McDonald, J. S., Kallmes, D. F., Jentoft, M. E., Murray, D. L., Thielen, K. R., Williamson, E. E., & Eckel, L. J. (2015). Intracranial gadolinium deposition after contrast-enhanced MR imaging. *Radiology*, *275*(3), 772–782. https://doi.org/10.1148/radiol.15150025

Mo, H., Fu, C., Wu, Z., Liu, P., Wen, Z., Hong, Q., Cai, Y., & Li, G. (2020). IL-6-targeted ultrasmall superparamagnetic iron oxide nanoparticles for optimized MRI detection of atherosclerotic vulnerable plaques in rabbits. *RSC Advances*, *10*(26), 15346–15353. https://doi.org/10.1039/c9ra10509c

Na, H. B., & Hyeon, T. (2009). Nanostructured T_1 MRI contrast agents. *Journal of Materials Chemistry*, *19*(35), 6267–6273. https://doi.org/10.1039/B902685A

Ni, D., Bu, W., Ehlerding, E. B., Cai, W., & Shi, J. (2017). Engineering of inorganic nanoparticles as magnetic resonance imaging contrast agents. *Chemical Society Reviews*, *46*(23), 7438–7468. https://doi.org/10.1039/c7cs00316a

Palacios-Hernandez, T., Diaz-Diestra, D. M., Nguyen, A. K., Skoog, S. A., Vijaya Chikkaveeraiah, B., Tang, X., Wu, Y., Petrochenko, P. E., Sussman, E. M., & Goering, P. L. (2020). Cytotoxicity, cellular uptake and apoptotic responses in human coronary artery endothelial cells exposed to ultrasmall superparamagnetic iron oxide nanoparticles. *Journal of Applied Toxicology*, *40*(7), 918–930. https://doi.org/10.1002/jat.3953

Pellico, J., Fernandez-Barahona, I., Benito, M., Gaitan-Simon, A., Gutierrez, L., Ruiz-Cabello, J., & Herranz, F. (2019). Unambiguous detection of atherosclerosis using bioorthogonal nanomaterials. *Nanomedicine: Nanotechnology, Biology and Medicine*, *17*, 26–35. https://doi.org/10.1016/j.nano.2018.12.015

Pombo-García, K., Rühl, C., Lam, R., Barreto, J. A., Ang, C.-S., Scammells, P. J., Comba, P., Spiccia†, L., Graham, B., Joshi, T., & Stephan, H. (2017). Zwitterionic modification of ultrasmall iron oxide nanoparticles for reduced protein corona formation. *ChemPlusChem*, *82*(4), 638–646. https://doi.org/10.1002/cplu.201700052

Qiao, R., Huang, X., Qin, Y., Li, Y., Davis, T. P., Hagemeyer, C. E., & Gao, M. (2020). Recent advances in molecular imaging of atherosclerotic plaques and thrombosis. *Nanoscale*, *12*(15), 8040–8064. https://doi.org/10.1039/d0nr00599a

Qiao, R. R., Yang, C. H., & Gao, M. Y. (2009). Superparamagnetic iron oxide nanoparticles: From preparations to in vivo MRI applications. *Journal of Materials Chemistry*, *19*(35), 6274–6293. https://doi.org/10.1039/b902394a

Reaney, S. H., Bench, G., & Smith, D. R. (2006). Brain accumulation and toxicity of Mn(II) and Mn(III) exposures. *Toxicological Sciences*, *93*(1), 114–124. https://doi.org/10.1093/toxsci/kfl028

Ruetten, P. P. R., Cluroe, A. D., Usman, A., Priest, A. N., Gillard, J. H., & Graves, M. J. (2020). Simultaneous MRI water-fat separation and quantitative susceptibility mapping of carotid artery plaque pre- and post-ultrasmall superparamagnetic iron oxide-uptake. *Magnetic Resonance in Medicine*, *84*(2), 686–697. https://doi.org/10.1002/mrm.28151

Rui, Y. P., Liang, B., Hu, F. L., Xu, J., Peng, Y. F., Yin, P. H., Duan, Y., Zhang, C., & Gu, H. C. (2016). Ultra-large-scale production of ultrasmall superparamagnetic iron oxide nanoparticles for T_1-weighted MRI. *RSC Advances*, *6*(27), 22575–22585. https://doi.org/10.1039/c6ra00347h

Saito, S., Tsugeno, M., Koto, D., Mori, Y., Yoshioka, Y., Nohara, S., & Murase, K. (2012). Impact of surface coating and particle size on the uptake of small and ultrasmall superparamagnetic iron oxide nanoparticles by macrophages. *International Journal of Nanomedicine*, *7*, 5415–5421. https://doi.org/10.2147/IJN.S33709

Sandiford, L., Phinikaridou, A., Protti, A., Meszaros, L. K., Cui, X., Yan, Y., ... Rosales, R. T. M. d. (2013). Bisphosphonate-anchored PEGylation and radiolabeling of superparamagnetic iron oxide: Long-circulating nanoparticles for *in vivo* multimodal (T_1 MRI-SPECT) imaging. *ACS Nano*, *7*(1), 500–512. https://doi.org/10.1021/nn3046055

Shen, Z., Chen, T., Ma, X., Ren, W., Zhou, Z., Zhu, G., Zhang, A., Liu, Y., Song, J., Li, Z., Ruan, H., Fan, W., Lin, L., Munasinghe, J., Chen, X., & Wu, A. (2017). Multifunctional theranostic nanoparticles based on exceedingly small magnetic iron oxide nanoparticles for T_1-weighted magnetic resonance imaging and chemotherapy. *ACS Nano*, *11*(11), 10992–11004. https://doi.org/10.1021/acsnano.7b04924

Shen, Z., Wu, A., & Chen, X. (2017). Iron oxide nanoparticle based contrast agents for magnetic resonance imaging. *Molecular Pharmaceutics*, *14*(5), 1352–1364. https://doi.org/10.1021/acs.molpharmaceut.6b00839

Sherwood, J., Rich, M., Lovas, K., Warram, J., Bolding, K. M., & Bao, Y. (2017). T_1-enhanced MRI-visible nanoclusters for imaging-guided drug delivery. *Nanoscale*, *9*(32), 11785–11792. https://doi.org/10.1039/c7nr04181k

Zou, Y., Li, D., Wang, Y., Ouyang, Z., Peng, Y., Tomás, H., Xia, J., Rodrigues, J., Shen, M., & Shi, X. (2020). Polyethylenimine nanogels incorporated with ultrasmall iron oxide nanoparticles and doxorubicin for MR imaging-guided chemotherapy of tumors. *Bioconjugate Chem*, *31*(3), 907–915. https://doi.org/10.1021/acs.bioconjchem.0c00036

Shin, T.-H., Choi, J. S., Yun, S., Kim, I. S., Song, H. T., Kim, Y., Park, K. I., & Cheon, J. (2014). T_1 and T_2 dual-mode MRI contrast agent for enhancing accuracy by engineered nanomaterials. *ACS Nano*, *8*(4), 3393–3401. https://doi.org/10.1021/nn405977t

Shin, T.-H., Choi, Y., Kim, S., & Cheon, J. (2015). Recent advances in magnetic nanoparticle-based multi-modal imaging. *Chemical Society Reviews*, *44*(14), 4501–4516. https://doi.org/10.1039/c4cs00345d

Shin, T.-H., Kim, P. K., Kang, S., Cheong, J., Kim, S., Lim, Y., Shin, W., Jung, J. Y., Lah, J. D., Choi, B. W., & Cheon, J. (2021). High-resolution T_1 MRI via renally clearable dextran nanoparticles with an iron oxide shell. *Nature Biomedical Engineering*, *5*(3), 252–263. https://doi.org/10.1038/s41551-021-00687-z

Simon, G. H., von Vopelius-Feldt, J., Wendland, M. F., Fu, Y., Piontek, G., Schlegel, J., Chen, M. H., & Daldrup-Link, H. E. (2006). MRI of arthritis: Comparison of ultrasmall superparamagnetic iron oxide vs. Gd-DTPA. *Journal of Magnetic Resonance Imaging*, *23*(5), 720–727. https://doi.org/10.1002/jmri.20556

Smits, L. P., Tiessens, F., Zheng, K. H., Stroes, E. S., Nederveen, A. J., & Coolen, B. F. (2017). Evaluation of ultrasmall superparamagnetic iron-oxide (USPIO) enhanced MRI with ferumoxytol to quantify arterial wall inflammation. *Atherosclerosis*, *263*, 211–218. https://doi.org/10.1016/j.atherosclerosis.2017.06.020

Song, X., Gong, H., Yin, S., Cheng, L., Wang, C., Li, Z., Li, Y., Wang, X., Liu, G., & Liu, Z. (2013). Ultra-small iron oxide doped polypyrrole nanoparticles for *in vivo* multimodal imaging guided photothermal therapy. *Advanced Functional Materials*, *24*(9), 1194–1201. https://doi.org/10.1002/adfm.201302463

Stanicki, D., Boutry, S. e., Laurent, S., Wacheul, L., Nicolas, E., Crombez, D., Vander Elst, L., Lafontaine, D. L. J., & Muller, R. N. (2014). Carboxy-silane coated iron oxide nanoparticles: A convenient platform for cellular and small animal imaging. *Journal of Materials Chemistry B*, *2*(4), 387–397. https://doi.org/10.1039/c3tb21480j

Sun, H., Zhang, B., Jiang, X., Liu, H., Deng, S., Li, Z., & Shi, H. (2018). Radiolabeled ultra-small Fe_3O_4 nanoprobes for tumor-targeted multimodal imaging. *Nanomedicine*, *14*(1), 5–17. https://doi.org/10.2217/nnm-2018-0219

Ta, H. T., Li, Z., Hagemeyer, C. E., Cowin, G., Zhang, S., Palasubramaniam, J., Alt, K., Wang, X., Peter, K., & Whittaker, A. K. (2017). Molecular imaging of activated platelets via antibody-targeted ultra-small iron oxide nanoparticles displaying unique dual MRI contrast. *Biomaterials*, *134*, 31–42. https://doi.org/10.1016/j.biomaterials.2017.04.037

Thrippleton, M. J., Blair, G. W., Valdes-Hernandez, M. C., Glatz, A., Semple, S. I. K., Doubal, F., Vesey, A., Marshall, I., Newby, D., & Wardlaw, J. M. (2019). MRI relaxometry for quantitative analysis of USPIO uptake in cerebral small vessel disease. *International Journal of Molecular Sciences*, *20*(3), 776. https://doi.org/10.3390/ijms20030776

Tromsdorf, U. I., Bruns, O. T., Salmen, S. C., Beisiegel, U., & Weller, H. (2009). A highly effective, nontoxic T_1 MR contrast agent based on ultrasmall PEGylated iron oxide nanoparticles. *Nano Letters*, *9*(12), 4434–4440. https://doi.org/10.1021/nl902715v

Usman, A., Sadat, U., Patterson, A. J., Tang, T. Y., Varty, K., Boyle, J. R., Armon, M. P., Hayes, P. D., Graves, M. J., & Gillard, J. H. (2015). Use of ultrasmall superparamagnetic iron oxide particles for imaging carotid atherosclerosis. *Nanomedicine*, *10*(19), 3077–3087. https://doi.org/10.2217/nnm.15.136

Wang, G., Gao, W., Zhang, X., & Mei, X. (2016). Au nanocage functionalized with ultra-small Fe_3O_4 nanoparticles for targeting T_1–T_2 dual MRI and CT imaging of tumor. *Scientific Reports*, *6*, 28258. https://doi.org/10.1038/srep28258

Wang, J., Jia, Y., Wang, Q., Liang, Z., Han, G., Wang, Z., Lee, J., Zhao, M., Li, F., Bai, R., & Ling, D. (2021). An ultrahigh-field-tailored T_1–T_2 dual-mode MRI contrast agent for high-performance vascular imaging. *Advanced Materials*, *33*(2), 2004917. https://doi.org/10.1002/adma.202004917

Wang, L., Huang, J., Chen, H., Wu, H., Xu, Y., Li, Y., Yi, H., Wang, Y. A., Yang, L., & Mao, H. (2017). Exerting enhanced permeability and retention effect driven delivery by ultrafine iron oxide nanoparticles with T_1−T_2 switchable magnetic resonance imaging contrast. *ACS Nano*, *11*(5), 4582–4592. https://doi.org/10.1021/acsnano.7b00038

Wang, P., Yang, J., Zhou, B., Hu, Y., Xing, L., Xu, F., Shen, M., Zhang, G., & Shi, X. (2017). Antifouling manganese oxide nanoparticles: Synthesis, characterization, and applications for enhanced MR imaging of tumors. *ACS Applied Materials & Interfaces*, *9*(1), 47–53. https://doi.org/10.1021/acsami.6b13844

Wei, H., Bruns, O. T., Kaul, M. G., Hansen, E. C., Barch, M., Wiśniowska, A., Chen, O., Chen, Y., Li, N., Okada, S., Cordero, J. M., Heine, M., Farrar, C. T., Montana, D. M., Adam, G., Ittrich, H., Jasanoff, A., Nielsen, P., & Bawendi, M. G. (2017). Exceedingly small iron oxide nanoparticles as positive MRI contrast agents. *Proceedings of the National Academy of Sciences of the United States of America*, *114*(9), 2325–2330. https://doi.org/10.1073/pnas.1620145114

Weng, Q., Hu, X., Zheng, J., Xia, F., Wang, N., Liao, H., Liu, Y., Kim, D., Liu, J., Li, F., He, Q., Yang, B., Chen, C., Hyeon, T., & Ling, D. (2019). Toxicological risk assessments of iron oxide nanocluster- and gadolinium-based T_1 MRI contrast agents in renal failure rats. *ACS Nano*, *13*(6), 6801–6812. https://doi.org/10.1021/acsnano.9b01511

Wu, T., Ding, X., Su, B., Soodeen-Lalloo, A. K., Zhang, L., & Shi, J. Y. (2018). Magnetic resonance imaging of tumor angiogenesis using dual-targeting RGD10-NGR9 ultrasmall superparamagnetic iron oxide nanoparticles. *Clinical Translational Oncology*, *20*(5), 599–606. https://doi.org/10.1007/s12094-017-1753-8

Xiao, W., Legros, P., Chevallier, P., Lagueux, J., Oh, J. K., & Fortin, M.-A. (2018). Superparamagnetic iron oxide nanoparticles stabilized with multidentate block copolymers for optimal vascular contrast in T_1-weighted magnetic resonance imaging. *ACS Applied Nano Materials*, *1*(2), 894–907. https://doi.org/10.1021/acsanm.7b00300

Xie, M., Wang, Z., Lu, Q., Nie, S., Butch, C. J., Wang, Y., & Dai, B. (2020). Ultracompact iron oxide nanoparticles with a monolayer coating of succinylated heparin: A new class of renal-clearable and nontoxic T_1 agents for high-field MRI. *ACS Applied Materials & Interfaces*, *12*(48), 53994–54004. https://doi.org/10.1021/acsami.0c12454

Xie, M., Xu, Y., Huang, J., Li, Y., Wang, L., Yang, L., & Mao, H. (2020). Going even smaller: Engineering sub-5 nm nanoparticles for improved delivery, biocompatibility, and functionality. *Wiley Interdisciplinary Reviews—Nanomedicine and Nanobiotechnolog*, *12*(6), 1644. https://doi.org/10.1002/wnan.1644

Xue, S., Zhang, C., Yang, Y., Zhang, L., Cheng, D., Zhang, J., Shi, H., & Zhang, Y. (2015). ^{99m}Tc-labeled iron oxide nanoparticles for dual-contrast (T_1/T_2) magnetic resonance and dual-modality imaging of tumor angiogenesis. *Journal of Biomedical Nanotechnology*, *11*, 1027–1037. https://doi.org/10.1166/jbn.2014.2023

Yang, C., Mi, X., Su, H., Yang, J., Gu, Y., Zhang, L., Sun, W., Liang, X., & Zhang, C. (2019). GE11-PDA-Pt@USPIOs nano-formulation for relief of tumor hypoxia and MRI/PAI-guided tumor radio-chemotherapy. *Biomaterials Science*, *7*(5), 2076–2090. https://doi.org/10.1039/c8bm01492b

Yang, H., Zhuang, Y., Sun, Y., Dai, A., Shi, X., Wu, D., Li, F., Hu, H., & Yang, S. (2011). Targeted dual-contrast T_1- and T_2-weighted magnetic resonance imaging of tumors using multifunctional gadolinium-labeled superparamagnetic iron oxide nanoparticles. *Biomaterials*, *32*(20), 4584–4593. https://doi.org/10.1016/j.biomaterials.2011.03.018

Yang, J., Luo, Y., Xu, Y., Li, J., Zhang, Z., Wang, H., Shen, M., Shi, X., & Zhang, G. (2015). Conjugation of iron oxide nanoparticles with RGD-modified dendrimers for targeted tumor MR imaging. *ACS Applied Materials & Interfaces*, *7*(9), 5420–5428. https://doi.org/10.1021/am508983n

Yin, J., Yao, D., Yin, G., Huang, Z., & Pu, X. (2019). Peptide-decorated ultrasmall superparamagnetic nanoparticles as active targeting mri contrast agents for ovarian tumors. *ACS Applied Materials & Interfaces*, *11*(44), 41038–41050. https://doi.org/10.1021/acsami.9b14394

Zeng, J., Jia, B., Qiao, R., Wang, C., Jing, L., Wang, F., & Gao, M. (2014). In situ ^{111}In-doping for achieving biocompatible and non-leachable ^{111}In-labeled Fe_3O_4 nanoparticles. *Chemical Communications*, *50*(17), 2170–2172. https://doi.org/10.1039/c3cc48948e

Zeng, J., Jing, L., Hou, Y., Jiao, M., Qiao, R., Jia, Q., Liu, C., Fang, F., Lei, H., & Gao, M. (2014). Anchoring group effects of surface ligands on magnetic properties of Fe_3O_4 nanoparticles: Towards high performance MRI contrast agents. *Advanced Materials*, *26*(17), 2694–2698. https://doi.org/10.1002/adma.201304744

Zeng, L., Wu, D., Zou, R., Chen, T., Zhang, J., & Wu, A. (2017). Paramagnetic and superparamagnetic inorganic nanoparticles for T_1-weighted magnetic resonance imaging. *Current Medicinal Chemistry*, *24*(25), 1–17. https://doi.org/10.2174/0929867324666170314124616

Zhang, N., Wang, Y., Zhang, C., Fan, Y., Li, D., Cao, X., Xia, J., Shi, X., & Guo, R. (2020). LDH-stabilized ultrasmall iron oxide nanoparticles as a platform for hyaluronidase-promoted MR imaging and chemotherapy of tumors. *Theranostics*, *10*(6), 2791–2802. https://doi.org/10.7150/thno.42906

Zhang, P., Zeng, J., Li, Y., Yang, C., Meng, J., Hou, Y., & Gao, M. (2021). Quantitative mapping of glutathione within intracranial tumors through interlocked MRI signals of a responsive nanoprobe. *Angewandte Chemie International Edition*, *60*(15), 2–11. https://doi.org/10.1002/anie.202014348

Zhao, X. L., Zhao, H. L., Chen, Z. Y., & Lan, M. B. (2014). Ultrasmall superparamagnetic iron oxide nanoparticles for magnetic resonance imaging contrast agent. *Journal of Nanoscience and Nanotechnology*, *14*(1), 210–220. https://doi.org/10.1166/jnn.2014.9192

Zhou, H., Ge, J., Miao, Q., Zhu, R., Wen, L., Zeng, J., & Gao, M. (2020). Biodegradable inorganic nanoparticles for cancer theranostics: Insights into the degradation behavior. *Bioconjugate Chemisty*, *31*(2), 315–331. https://doi.org/10.1021/acs.bioconjchem.9b00699

Zhou, H., Tang, J., Li, J., Li, W., Liu, Y., & Chen, C. (2017). *In vivo* aggregation-induced transition between T_1 and T_2 relaxations of magnetic ultra-small iron oxide nanoparticles in tumor microenvironment. *Nanoscale*, *9*(9), 3040–3050. https://doi.org/10.1039/c7nr00089h

Zhou, Z., Wang, L., Chi, X., Bao, J., Yang, L., Zhao, W., Chen, Z., Wang, X., Chen, X., & Gao, J. (2013). Engineered iron-oxide-based nanoparticles as enhanced T_1 contrast agents for efficient tumor imaging. *ACS Nano*, *7*(4), 3287–3296. https://doi.org/10.1021/nn305991e

Zhou, Z., Yang, L., Gao, J., & Chen, X. (2019). Structure-relaxivity relationships of magnetic nanoparticles for magnetic resonance imaging. *Advanced Materials*, *31*(8), 1804567. https://doi.org/10.1002/adma.201804567

How to cite this article: Chen, C., Ge, J., Gao, Y., Chen, L., Cui, J., Zeng, J., & Gao, M. (2022). Ultrasmall superparamagnetic iron oxide nanoparticles: A next generation contrast agent for magnetic resonance imaging. *Wiley Interdisciplinary Reviews: Nanomedicine and Nanobiotechnology*, *14*(1), e1740. https://doi.org/10.1002/wnan.1740